1-1-2013

Fabrication and Characterization of Surrogate Fuel Particles Using the Spark Erosion Method

Kathryn Elizabeth Metzger
University of South Carolina

Fabrication and Characterization of Surrogate Fuel Particles Using the Spark Erosion Method

by

Kathryn E. Metzger

Bachelor of Science
University of South Carolina, 2009

Submitted in Partial Fulfillment of the Requirements

For the Degree of Master of Science in

Nuclear Engineering

College of Engineering and Computing

University of South Carolina

2013

Accepted by:

Travis W. Knight, Major Professor

Elwyn Roberts, Committee Member

Lacy Ford, Vice Provost and Dean of Graduate Studies

ACKNOWLEDGEMENTS

This research was performed using funding received from the DOE Office of Nuclear Energy's Nuclear Energy University Programs (NEUP) in the form of a graduate fellowship.

Special thanks go to my advisor Dr. Travis W. Knight for the opportunity to join the University of South Carolina's Nuclear Engineering program and his research group. His support has been invaluable. I would also like to thank Dr. Elwyn Roberts for his review and meaningful suggestions during the process. Thanks to Dr. Kaoumi and my other professors for their education and guidance during my time thus far in the NE program at USC. I would also like to thank the other graduate students in my research group: Luke Hallman, Ian Porter, Seung Min Lee, Bo Shiuan Li, and Kyle Hrutkay for their aid in the completion of this work. Thanks also to Misty, Lalitha, and Renee for their smiles and words of encouragement.

Finally, I would like to express my heartfelt gratitude to my mother, father, nana, brother, and boyfriend for their love and support. I could not have accomplished this without their encouragement, prayers, and reassurance.

ABSTRACT

In light of the disaster at the Fukushima Daiichi Nuclear Plant, the Department of Energy's Advanced Fuels Program has shifted its interest from enhanced performance fuels to enhanced accident tolerance fuels. Dispersion fuels possess higher thermal conductivities than traditional light water reactor fuel and as a result, offer improved safety margins. The benefits of a dispersion fuel are due to the presence of the secondary non-fissile phase (matrix), which serves as a barrier to fission products and improves the overall thermal performance of the fuel. However, the presence of a matrix material reduces the fuel volume, which lowers the fissile content of dispersion. This issue can be remedied through the development of higher density fuel phases or through an optimization of fuel particle size and volume loading. The latter requirement necessitates the development of fabrication methods to produce small, micron-order fuel particles. This research examines the capabilities of the spark erosion process to fabricate particles on the order of 10 μm. A custom-built spark erosion device by CT Electromechanica was used to produce stainless steel surrogate fuel particles in a deionized water dielectric. Three arc intensities were evaluated to determine the effect on particle size. Particles were filtered from the dielectric using a polycarbonate membrane filter and vacuum filtration system. Fabricated particles were characterized via field emission scanning electron microscopy (FESEM), laser light particle size analysis, energy-dispersive spectroscopy (EDS), X-ray diffraction analysis (XRD), and gas pycnometry.

FESEM images reveal that the spark erosion process produces highly spherical particles on the order of 10 microns. These findings are substantiated by the results of particle size analysis. Additionally, EDS and XRD results indicate the presence of oxide phases, which suggests the dielectric reacted with the molten debris during particle formation.

TABLE OF CONTENTS

LIST OF TABLES

LIST OF FIGURES

List of Abbreviations

ADUN ..... Acid-Deficient Uranyl Nitrate

CCD ..... Charge-Coupled Device

CER-MET ..... Ceramic-Metallic

Cr_2FeO_4 ..... Chromium Iron Oxide (Chromite)

Cr_2NiO_4 ..... Chromium Nickel Oxide

CVD ..... Chemical Vapor Deposition

DC ..... Direct Current

DOE ..... Department of Energy

EDM ..... Electric Discharge Machining

EDS ..... Energy Dispersive Spectroscopy

EMC ..... Electron Microscopy Center

Fe_3O_4 ..... Iron (II, III) Oxide

Fe_2O_3 ..... Iron (III) Oxide

FeO ..... Iron (II) Oxide

FESEM ..... Field Emission Scanning Electron Microscope

HEU ..... Highly-Enriched Uranium

HMTA ..... Hexamethylenetetramine

HP ..... Horse Power

LEU ..... Low-Enriched Uranium

LWR.....Light Water Reactor

MET-MET ..... Metallic-Metallic

ORNL..... Oak Ridge National Lab

PMEDM.....Powder Mixed Electric Discharge Machining

R&D..... Research and Development

REP ..... Rotating Electrode Process

RERTR..... Reduced Enrichment Research and Test Reactor

RPM ..... Rotations Per Minute

ThO_2.....Thorium Dioxide

TD .....Theoretical Density

UO_2 ..... Uranium Dioxide

$(U,Pu)O_2$..... Uranium-Plutonium Dioxide

XRD .....X-Ray Diffraction

CHAPTER 1

INTRODUCTION AND MOTIVATION

The sustainability of the current Light Water Reactor (LWR) fleet is dictated by the ability to maintain safe and economic operation beyond the initially licensed reactor lifetime. The Department of Energy (DOE) Light Water Sustainability Program has a roadmap for the life extension of these reactors. Among the research and development (R&D) tasks identified, is the need to investigate advanced LWR fuels capable of achieving higher burnups [1]. In addition to reaching higher burnups, a candidate fuel must also guarantee a safety margin more competitive than existing UO2 fuel forms.

In March 2011, the events at Fukushima reinforced the need for fuels designed with increased accident tolerance. As a result, the interest of the DOE Advanced Fuels Program shifted from enhanced performance fuels to enhanced accident tolerance fuels. The DOE defines enhanced accident tolerance fuels as fuels that "in comparison with the standard UO2-Zircalloy system currently used by the nuclear industry, can tolerate loss of active cooling in the reactor core for a considerably longer time period (depending on the LWR system and accident scenario) while maintaining or improving the fuel performance during normal operations, operational transients, as well as design-basis and beyond design-basis events" [1].

Dispersion fuels are attractive because their higher melting temperatures and thermal conductivities offer improved safety margins. The presence of matrix materials, regardless of whether they are metallic or ceramic in nature tends to reduce fuel operating temperatures and fission gas release. A matrix is also a proven barrier to fission products. Therefore, a dispersion fuel in which fuel particles are embedded in a matrix material is an inherently safer fuel design. Among the fuel types being investigated are Ceramic fuel-metallic matrix (Cer-Met), Metallic fuel-metallic matrix (Met-Met), and Metallic Fuels.

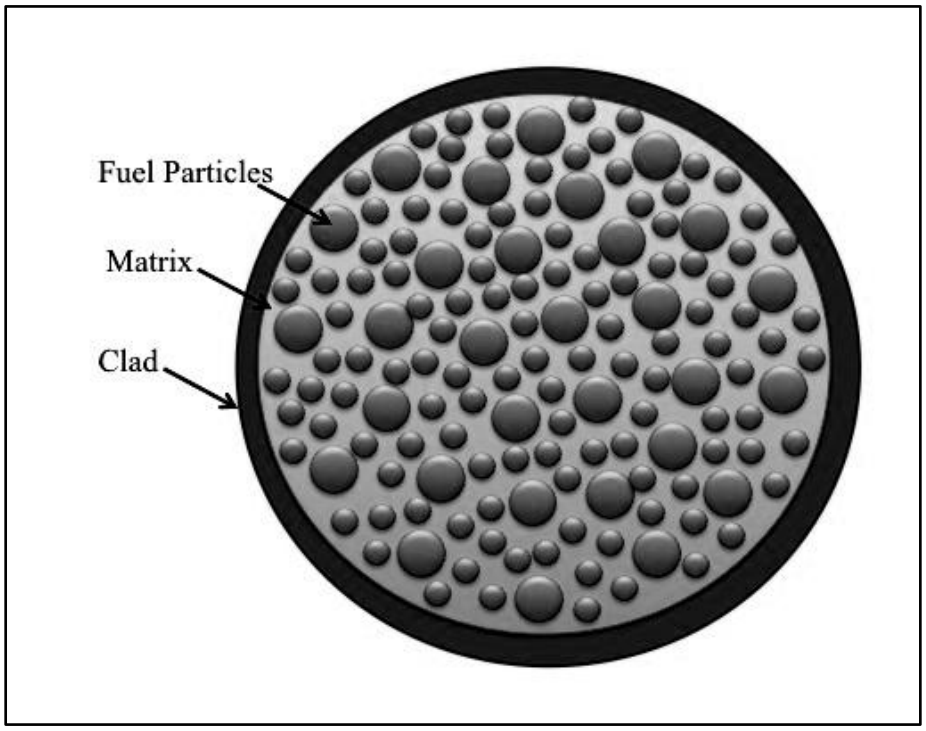

Figure 1.1: Cross section of a dispersion fuel. Fuel particles constitute the fissile phase and are embedded in a nonfissionable matrix material.

By suspending fuel particles within an inert matrix, the volume of fuel and overall fissile content is significantly decreased. This is one of the greatest challenges presented by dispersion fuels. However, this can be mitigated by selecting fuel phases with higher

uranium density or by increasing the enrichment of the fuel. Enrichment of the fuel beyond regulatory limits is not a viable option if fuels are intended for use in current LWRs. Instead, the need for increased enrichment can be overcome through the selection of a new fuel phase with high uranium content. Another means of increasing the fissile content in the dispersion is by increasing the fuel-loading fraction within the matrix. This is accomplished through an optimization of fuel and matrix particle size distributions. The packing fraction is governed by the size distribution of the constituent particles and the greatest volume loading is achieved when multiple particle sizes are employed.

The loading fraction increases with the ratio of large to small particle diameters. McGeary investigated the idealized packing of mechanical spheres in single component, binary, ternary, and quaternary systems [2]. For binary systems, it was determined that the maximum or limit for void efficiency occurred when the ratio of large particle diameter to small particle diameter was 10. For example, a combination of 100-micron and 10-micron particles would produce a highly dense dispersion. Any further increases in this ratio did not substantially increase the packing density. For ternary component systems, McGeary found that the maximum density was achieved for particles with a size ratio 77:7:1 in a volume percentage of 66:25:9, respectively. Subtle shifts in the size ratio and the particle size distribution will provide increased voids, which can be beneficial should an initial degree of fuel porosity be desired. Thus, the development of dispersion fuels will require a formal understanding of mechanical particle loading as well as size-specific particle fabrication methods.

Traditional fuel particle production techniques like ball milling may be an unsuitable fabrication method given the pyrophoric nature of many proposed fuel phases.

The Sol-gel method is an alternative fabrication process that produces highly spherical particles of consistent size. This would be an ideal choice for particle production; however, the process generates a large quantity of mixed waste and more importantly, cannot be used to produce particles below 50 μm [3]. Therefore, an alternative fabrication route must be used to achieve smaller-sized particles.

Spark erosion can be used to produce highly spherical particles ranging in size from a few nanometers to a several hundred micrometers [4]. The term spark erosion encompasses all machining processes in which a spark is generated between two electrodes submerged in a dielectric medium. Electric discharge machining is the most common form of spark erosion and has been used for decades to machine hard and brittle materials into complex shapes and dies. Spark erosion is also a very versatile process that can be used to produce particles of varying sizes from any moderately conductive workpiece.

This research seeks to evaluate the spark erosion process for the fabrication of particles smaller than achievable through the sol-gel processes. Specifically, it was desired to determine the parameters necessary to generate microspheres on the order of 10 μm. To accomplish this, a custom-built spark erosion device by CT Electromechanica of Argentina was used to fabricate surrogate fuel microspheres. The chosen diameter of 10 μm is a nominal value intended only to validate the use of spark erosion for micron-order particle applications. Additionally, by isolating a specific particle diameter, it was possible to evaluate the difficulty of producing a narrow and reproducible size distribution. A literature review was conducted to guide in the selection of the starting experimental parameters. Fabricated particles were characterized using field scanning

electron microscopy, energy dispersive X-ray spectroscopy, X-Ray diffraction analysis, particle yield analysis, laser light particle size analysis, and helium gas pycnometry.

The results of the research reveal that the spark erosion process is an effective means of producing highly spherical particles on the order of 10 μm. The size distribution of particles produced using the spark erosion method is dominated by a large particle size but also shows the presence of much smaller particles. Repeated filtrations of the spark eroded particles in the dielectric medium would allow for a greater degree of particle separation and could isolate the 10 μm, larger particles, if desired.

Compositional analysis using X-ray diffraction and energy dispersive x-ray spectroscopy revealed high oxygen levels in the fabricated particles. The presence of oxide phases in the surrogate particles is due to the interaction of the molten debris with dielectric during solidification. Because deionized water was used as the dielectric, oxide phases were formed. The selection of a different dielectric, like a hydrocarbon would change the phases identified. Gas pycnometry measurements show that the particles have a density less than both the starting 304SS workpiece and the identified XRD phases. This suggests that the particles have a porous structure, which could be confirmed through additional investigation.

CHAPTER 2

DISPERSION FUELS

A dispersion fuel is a nuclear fuel that consists of fissionable fuel particles dispersed in non-fissionable metallic, ceramic, or graphite medium [5]. The host material surrounding the fuel particles is referred to as the matrix. The motivation behind a dispersion fuel is that it combines the beneficial properties of the matrix material with the fissile characteristics of the particle fuel. A chosen matrix will support carbide, oxide, mixed oxide, nitride, ceramic, or even alloy fuel particles. One of the advantages of a dispersion fuel is the ability to optimize mechanical properties and performance by selecting an appropriate fuel composition. The performance and power density can be influenced by fuel particle size, geometry, and volume fraction. Thus, a dispersion fuel can effectively be designed for the needs of any specific application.

The use of dispersion fuels dates back to the 1950's. At the time, dispersion fuels were seen as an ideal candidate for research and test reactors. Due to their robust performance capabilities, dispersion fuels have also been investigated for use in space nuclear power systems, advanced reactor systems capable of waste transmutation, and even in current LWRs seeking to increase burnup [6].

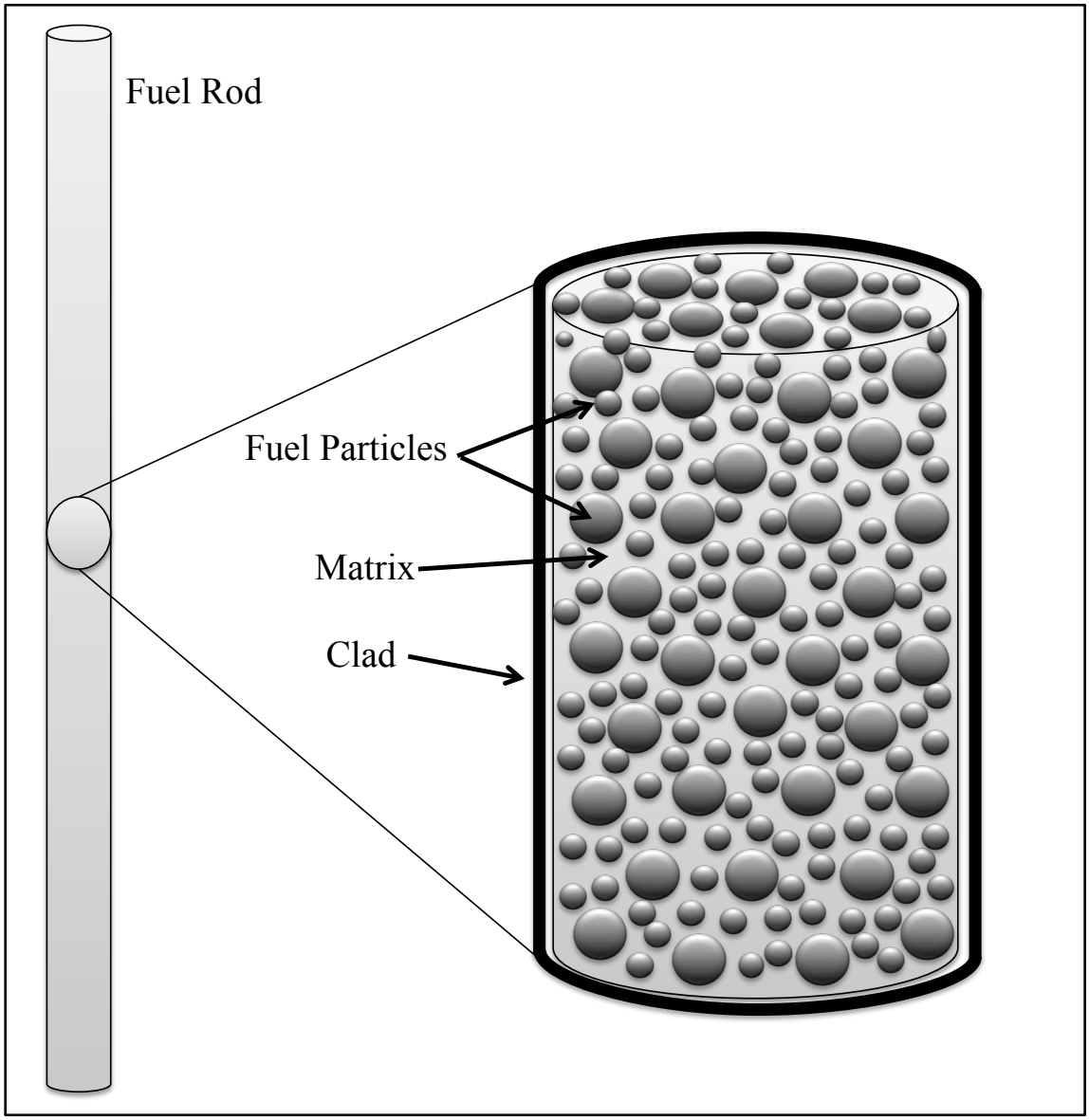

Figure 2.1: Example of a rod shaped dispersion fuel. Fissile particles are embedded within a nonfissionable matrix.

2.1 History and Background

The development of dispersion fuels gained traction in the 1950s and 1960s with the design of Aluminum-based dispersion fuels for research reactors. Fuel forms investigated included UAl_3, U_3O_8, and U_3Si_2 [5]. Such Aluminum based dispersion fuels are common in most research and test reactors in use today. The U.S. reduced

enrichment research and test reactor (RERTR) program, which began in 1978, saw a renewed interested in dispersion fuels. The motivation for the RERTR program was to address a nonproliferation goal and quell concerns about certain fuels providing an easy route to the acquisition of nuclear weapons. The RERTR program examined the feasibility of a transition from the use of highly enriched uranium (HEU) to low enriched uranium (LEU) fuels in research and test reactors. Enrichment to less than 20% U^{235} is internationally recognized as a complete barrier to weapons usability [7]. A simple substitution across the board for LEU in existing fuel designs would reduce the core performance. An LEU replacement in existing fuel designs would reduce the core reactivity, increase fuel costs, decrease U^{235} burnup capability, and decrease the flux-per-unit-power in the reactor [7]. Therefore, the challenge presented was to pack the same amount of U^{235} formerly in HEU fuel into fuel utilizing LEU without changing the dimensions of the fuel element, and while maintaining the same power density [8]. In order to accomplish such a task, new fuels were developed that maintained approximately the same amount of U^{235}, despite the decreased enrichment. There are three ways to increase the uranium loading in the fuel element: increase the enrichment of the uranium in the fuel, increasing the actual uranium density in the fissile phase, or increase the volume of the fissile material relative to the matrix. The first option, increased enrichment, is not feasible for LWR applications. The development of fuels with higher uranium density will benefit many applications. Table 2.1 shows a list of proposed fuel phases, which were examined specifically during the RERTR program.

Table 2.1: The following is a list of proposed fuel particle phases examined during the RERTR program. [9]

Fuels with High Uranium Density		
Compound	**Density, g/cm^3**	**U density, g/cm^3**
UO_2	11.0	9.7
U_3Si_2	12.2	11.3
UB_2	12.7	11.6
UCo	15.4	12.3
UC	13.6	13.0
UN	14.3	13.5
U_2Ti	15.1	13.7
U_2Mo	16.6	13.8
U_2Tc	16.8	13.9
U_2Ru	16.9	13.9
U_3Si	15.5	14.6
U_6Co	17.7	17.0
U_6Ni	17.6	16.9
U_6Fe	17.7	17.0
U_6Mn	17.8	17.1
Alloy (given in wt%)	**Density, g/cm^3**	**U density, g/cm^3**
U-9Mo	17.0	15.5
U-5Mo	17.9	17.0
U-3Zr-9Nb	16.2	14.3
U-4Zr-2Nb	17.3	16.3

In addition to exploring fissile materials or alloys with higher uranium densities, it is also possible to increase the fuel particle volume fraction within the matrix. This can be accomplished by selecting an ideal fuel particle size distribution.

More recently, dispersion fuels have been revisited by the Department of Energy's Light Water Reactor Sustainability program in an attempt to study the possible use of dispersion fuels with enhanced accident tolerance capabilities for deployment in the current light water reactor fleet. The goal of enhanced accident tolerance was born

out of the accident at Fukushima and recognition that future fuel designs must perform as well if not better than the current industry standard in the event of beyond-design basis accidents. Dispersion fuel is an attractive candidate for the enhanced accident tolerance fuels program because its higher melting temperatures and thermal conductivities offer improved safety margins. Historically, dispersion fuels have often taken the form of fuel plates. However, it is possible to use dispersion fuels in the form of traditional pellets so that they can be used in current LWRs. Whether they feature a ceramic or metallic fuel phase, a dispersion that utilizes a metallic matrix, so-called CER-METs and MET-METs, are viable fuel candidates for use in fast reactors as well as current LWRs [10]. The use of a Zirconium or Aluminum metallic matrix ensures low centerline operating temperatures and provides better safety margins under power ramp and accident conditions.

2.2 Overview and Benefits

The matrix material can be selected such that it offers improved strength, increased radiation stability, and high thermal conductivity [11]. The matrix is usually a metal or an alloy. This allows for high power densities and low failure consequences [6]. By isolating the fuel particles, a substantial volume of the matrix remains undamaged by fission products [5]. This allows the fuel to reach higher burnups than would be possible in traditional ceramic fuel. Of course, fuel particle, matrix, and cladding materials should be selected bearing in mind the potential interaction between the phases in high temperature and accident scenarios.

Because traditional Uranium Dioxide (UO_2) fuel has poor thermal conductivity, a large temperature gradient is seen across the fuel. This gradient is amplified for high

linear heating rates and is pronounced during thermal excursions like startup. This temperature gradient causes the center of the fuel to expand more rapidly than the pellet's periphery. Such thermal stresses deform the pellet until the fuel fracture stress is exceeded. When the fracture stress is exceeded, the brittle UO_2 pellet cracks. Cracking of the fuel pellet further reduces the effective thermal conductivity of the fuel. This translates to the fuel's centerline being unable to transfer heat. This leads to an increased centerline temperature. Additionally, cracks allow for the migration of fission gases to migrate to the pellet-clad gap. Fission gases, like Krypton and Xenon, have lower thermal conductivities than the helium fill gas and reduce heat transfer across the gap. Solid fission fragments as well as fission gases cause fuel swelling. Solid fragments can cause expansion of the fuel matrix while the fission gas atoms that are released into the fuel-clad gap, exert additional pressure on the cladding. In extreme operating conditions, or accident scenarios, stressed cladding may rupture.

In contrast, metallic-matrix dispersion fuels feature fuel particles surrounded by a highly conductive metal. The high thermal conductivity of the metal reduces the temperature gradient across the fuel pellet, thereby improving the heat transfer and performance of the fuel. A lower operating temperature and temperature gradient means the robust fuel will have improved safety margins in the event of an accident. Additionally, by containing the fuel to spheres dispersed in the matrix, fission fragment damage is localized to the microspheres. While this does result in a small ring of damage around the spheres, a large portion of the matrix remains interconnected and undamaged. This allows the fuel to maintain its dimensional stability and strength.

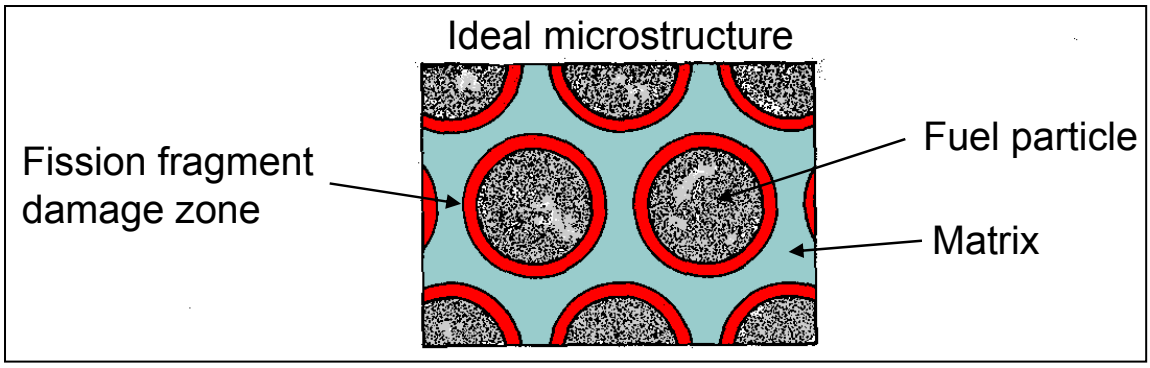

Figure 2.2: Fission fragment damaged is localized in a small ring around the fuel particle. This allows the supporting matrix material to remain interconnected and thus maintain its dimensional stability and strength. [6]

Matrix materials can be selected based on desired mechanical properties and ease of fabrication. Metallic matrix materials like aluminum and zirconium, offer high thermal conductivities, which lower the operating fuel temperature. Fuel particle composition can be selected based on the requirements of a given application. By substituting monolithic UO_2 pellet fuel for a dispersion of UO_2 particles in a zirconium matrix, a burnup equivalent to 85GWd/t in UO_2 pellet fuel can be achieved [6]. Thus, a dispersion fuel form can increase accident tolerance and enhance performance if used in current LWRs.

2.2.1 Fuel Volume Fraction

Volume loading is dependent upon the size of the fuel particles as well as the matrix particles. By utilizing binary, ternary, or even quaternary packing, it is possible to design a dispersion fuel with optimum matrix, void, and fuel phase fractions for a specified task. The ratio of diameters of matrix and fuel particles will influence the void volume in the fuel. In cases where fuel swelling is prone, it is desirable to fabricate the fuel with an initial porosity capable of offsetting the swelling. Particle size ratio is also important in maximizing the fuel phase loading in a dispersion fuel. Dispersions naturally have a smaller fissile phase volume than traditional monolithic fuels.

Therefore, in order to achieve a competitive fissile content, the fissile density must be maximized. The particle size of the fuel relative to the matrix, for the case of binary packing, will determine the possible fuel densities. In other cases, it is desirable to use two or more particle sizes for the fuel phase.

McGeary's research [2] on the mechanical packing of spherical particles followed the 1931 work of Furnas [12]. Furnas initiated the study of idealized packing of spheres of different sizes. McGeary's research substantiated Furnas' theories with experimental results. Specifically, the maximum density possible for a single-component, binary, ternary, and quaternary system was addressed. In the case of single component packing, particle size has no bearing on the packed density. The density of a single component packing is usually between 60% and 64% volume. However, the container size relative to particle diameter has a pronounced effect on packing density. McGeary found that the maximum density, a value of 62.5% theoretical density (TD), can be achieved when the ratio of the container diameter to that of the particle is greater than 200 [2]. However, the onset of the 62.5% TD value occurs at a much smaller ratio. Values of 61% and 62% TD can be seen as early as a container to particle diameter ratio of 10. For binary systems, it is obvious that the smaller the diameter of the fine spheres, the greater the density of the packing. The maximum achievable packing begins when the ratio of larger spheres to smaller spheres is approximately 10. Below 7, the density falls off rapidly. As the fraction of each sphere size in the mixture changes, the maximum achievable percentage of the theoretical density will also change. However, there are instances in which a specific phase density, or volume fraction, is more important than the overall

mixture density. Thus, it is important to know the desired properties of the mixture so that both mixture density and phase fraction can be optimized.

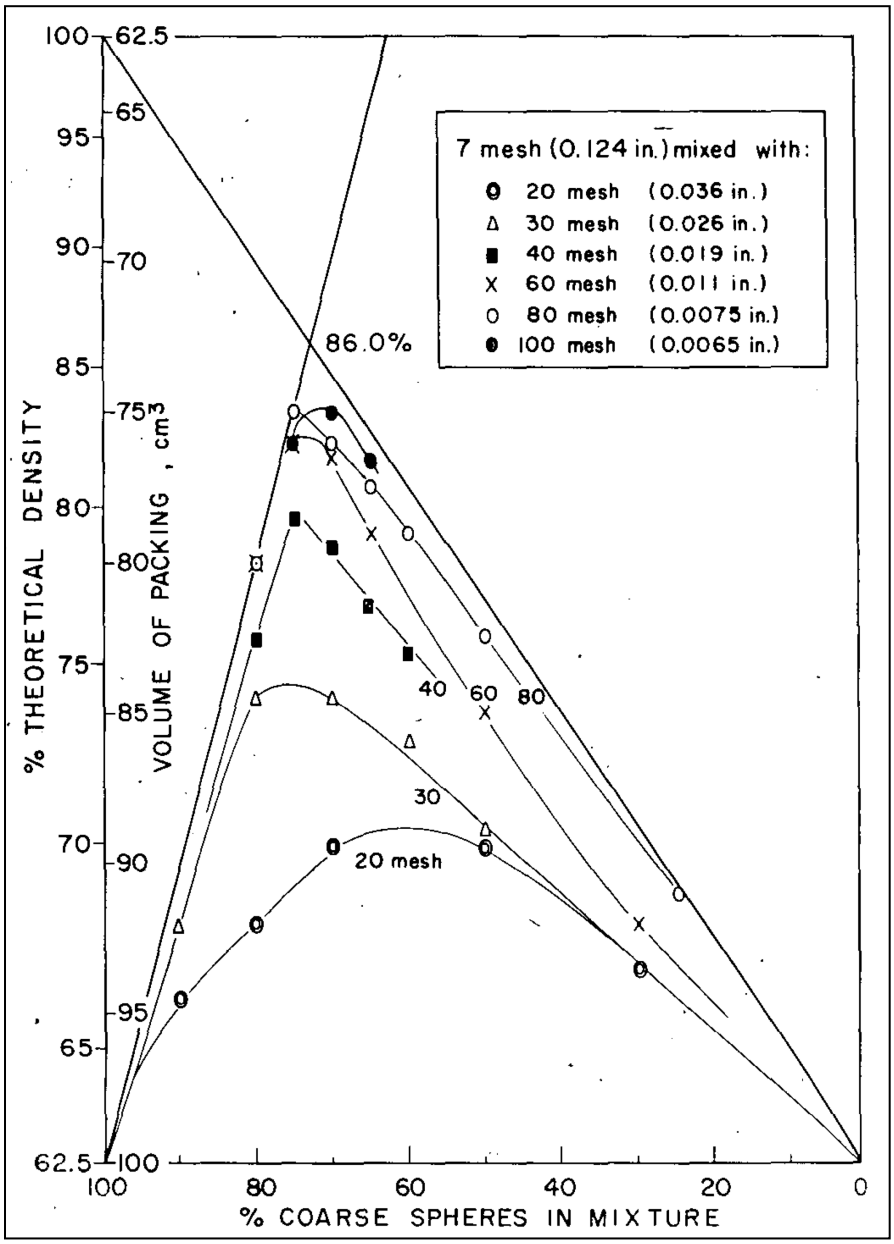

Figure 2.3: Binary packing of spheres. The fraction of theoretical density is shown for 20, 30, 40, 60, 80, and 100 mesh particles mixed with 7 mesh spheres. The theoretical density is a function of the fraction of coarse spheres (7 mesh) in the mixture. [2]

For ternary loadings, McGeary found that the maximum density occurred at volume percentages 66:25:9 (coarse, medium, and fine particles, respectively) in the size

ratio 77:7:1. Experimental results confirmed that this packing resulting in a density of 90% TD. Packing systems with four or more particle sizes increase the options for heterogeneous component loading. However, in terms of the overall mixture density, the benefit of each additional size was found to be only one-half that of the proceeding component.

Table 2.2: This table, reproduced from McGeary, illustrates the increase in TD with each additional component (particle size) [2].

Density of a Quaternary Packing									
				Composition				% of Theoretical Density	
Component	Mesh	*d*	*d* ratio	X_1	X_2	X_3	X_4	Calculated Limit	Experimental
1		0.505	316	1.00	---	---	---	60.5	58.0
2	14	0.061	38	0.726	0.274	---	---	85.9	80.0
3	60	0.011	7	0.647	0.244	0.109	---	94.2	89.8
4	400	0.0016	1	0.607	0.230	0.102	0.061	97.5	95.1

While a higher fuel volume fraction does increase the fissile content in the matrix, it can also increase the amount of irradiation swelling that the fuel pellet experiences [13]. Finlay et al. noted that this phenomenon was not pronounced in stable fuels with low swelling rates such as U_3Si_2. However, for less stable fuels like U_3Si, U_3SiAl, and U_6Fe, a larger fuel volume fraction increases the amount of swelling that occurs in the pellet. In order to optimize the performance of a dispersion fuel, it is necessary that appropriate fuel particle size(s) and matrix particle size be selected such that void volume and fissile phase density are guaranteed in terms of the desired composition.

2.2.2 Particle Size

Fuel particle size also impacts a dispersion fuel's thermomechanical performance. Ding et al. performed a series of three-dimensional finite element simulations on a UO_2-Zirconium dispersion fuel plate in order to examine the interaction between the fuel particle and matrix [14]. More specifically, the thermo-elastic performance of the fuel

was modeled as a function of particle size. It was determined that the fuel plate internal temperatures increase with increasing fuel particle diameters. At the interface between the fuel particle and the matrix, the von Mises stress increases with an increasing fuel particle diameter. The maximum von Mises stress within the fuel particle increases with increasing particle diameter, as well. Jiang et al. simulated the effect of a heterogeneous fuel particle loading in dispersion fuel rods. The results showed that the highest temperatures within the fuel were located close to the mid-plane of the fuel rod and at points where there was the smallest distance between fuel particles. However, the actual difference in temperatures values between particles from a performance standpoint was insignificant (less than 0.5 K variation). Thus, it was determined that for metallic matrices, the fuel particle-to-particle distance does not affect the maximum temperature in the fuel [15]. This is due to the high thermal conductivity of the metallic matrix.

2.3 Fabrication

The simplest method for manufacturing dispersion fuel follows the powder metallurgy process. Prefabricated fuel microspheres are mixed with a matrix material in powder form, and sintered into pellets or other desired shapes [16]. Sintering removes voids and pores in the fuel that can have a negative impact on heat conduction on and matrix fracture toughness. Matrix materials with high melting temperatures are desired for higher safety operating margins. However, this also presents a challenge in terms of sintering fuels to high densities because the task may involve several high temperature, long duration heating cycles. This issue is especially difficult when the fissile phase and the matrix material have different melting temperatures. There are many variations to this fabrication process; the silicide dispersion fuel work conducted at the A.A. Bochvar

Institute used capillary impregnation to draw molten matrix material up and around fuel particles previously vibro-loaded in a cladding [17]. Fuel particle production methods are discussed in the following sections.

2.3.1 Milling

In the case of Uranium aluminides or uranium silicides, the dispersed phase is produced by induction melting and casting. For brittle materials, the fabricated ingots can be comminuted to powder using hammer milling or ball milling techniques. This yields a fuel powder composed of small fuel particles, which is suitable in most dispersion fuels. However, tougher materials like U_3Si_2 required additional machining or crushing and yield "chips" rather than powder. Another problem with milling techniques is that the process increases the opportunity for foreign debris to contaminate the fuel particles. For highly reactive fuels, milling cannot be used due to the reactive nature of the particle with air.

2.3.2 Internal Gelation

The internal gelation process, or sol gel, offers several advantages to traditional milling. The aqueous process is capable of producing highly spherical particles with a reproducible size distribution. This method can be used to ceramic particle fuels, such as UO_2, $(U,Pu)O_2$, ThO_2, and even ceramics with minor actinide additives. Recently, ORNL has successfully extended the process to produce metal oxide spheres of titanium, zirconium, and iron. A drawback to the process is the large quantity of liquid waste generated. In the sol gel process, chilled clear broth droplets containing acid-deficient uranyl nitrate (ADUN), hexamethylenetetramine (HMTA), and urea are heated causing a homogenous gelation and solidification of the droplets. The particles assume a highly spherical shape due to the surface tension of the broth droplet. Following gelation and

solidification, the particles are washed and can be calcined and sintered to ceramic kernels of a desired density [18]. The sol gel process allows for the precise control of fuel composition, particle size, and density. The particle diameter is directly dependent upon the size of the both droplets, which can be easily fixed using a high frequency needle for deposition [18]. Thus, the process is capable of producing highly spherical particles within a narrow size distribution. The sol gel process has proven very successful in terms of producing particles on the order of 100-1000 μm. However, Vaidya et al. documented that the process is incapable of producing particles smaller than 50 μm [3]. Oak Ridge National Lab (ORNL) found that particle size was dependent on both needle frequency and the inner diameter of the broth-dispensing needle [18]. Generally, it was found that the diameter of the broth jet should be about one half the intended drop diameter. With a decreasing needle cavity, it eventually becomes impossible to flow the broth through the needle. This applies a lower limit to the size of fuel particles that can successfully be fabricated using the sol gel method.

2.3.3 Spark Erosion

Spark erosion can be used to produce highly spherical microparticles for use in dispersion fuels. Particles can be fabricated from any conductive material. Thus, the process can be used to produce the fuel particles as well as the stock powder for the matrix. In spark erosion, a spark is generated between two electrodes immersed in a dielectric fluid. Following the creation and breakdown of plasma between the two electrodes, molten material is ejected from the surface of the electrode and is rapidly quenched in the dielectric [1]. Metallic, alloy, and compound particles can be produced using this method with particles sizes ranging from on the order of nanometers up to hundreds of micrometers. Particle size and size distribution is dependent upon the

applied current, current frequency, and a number of other parameters [19]. Methods in which one or both of the electrodes rotate are referred to as a rotating electrode mechanism. Although most spark erosion devices feature a rotating electrode, the unique advantage associated with the rotating electrode processes seems limited to systems in which the is electrode sees thousands of rotations per minute (rpm). In this case, a high frequency of rotation is responsible for the smaller particle sizes associated with the method. Although spark erosion devices may feature a rotating electrode, it rotates with a much lower frequency of rotation. This low rotation frequency is responsible for clearing the debris from the gap between the electrodes, rather than directly influencing particle size. Although the rotating electrode process is capable of producing smaller particles than a classical spark erosion mechanism, the spark erosion mechanism is still capable of producing particles on the scale of several nanometers. A detailed review of the supporting science of spark erosion and the influence of process parameters on particle size and will be discussed in the next chapter.

CHAPTER 3

REVIEW OF SPARK EROSION MACHINING

3.1 HISTORY AND USE OF SPARK EROSION IN INDUSTRY

The first use of machining with electric discharge was during the 1930's. Henry Harding of Elox US developed a "disintegrator" to remove broken taps, studs, and bolts from valuable workpiece materials [20]. The cutting action of the disintegrator was accomplished by a series of intermittent electric arcs between a tool electrode and workpiece, which was connected to a DC power supply. Although the process was not precise and process parameters were not well understood, the disintegrator accomplished the task of material erosion and bit retrieval. In 1943, B. R. Lazarenko studied the prevention of wear on tungsten electrical contacts [21]. The research found that erosion was more precisely controlled when electrodes were immersed in a dielectric medium. By introducing the concept of controlled discharge conditions, this work initiated the development of advanced electric discharge machining with precision machining capabilities. Following Lazarenko's work, electric discharge technology developed rapidly. Today, the technology exhibits several variations and is used in a number of manufacturing applications including die and mold making, finishing, micro-machining, and particle production.

Within the literature, the terms “spark erosion machining” and “electric discharge machining (EDM)” are used interchangeably. However, there is a tendency to use EDM to discuss precision machining of a workpiece material, as in the case of die making. On the other hand, the powder and particle industry prefers the term spark erosion machining or rotating electrode machining, depending upon the specified process. In either case, the science and guiding principles discussed in the following section are the same.

Spark erosion has greatly increased the machinability of otherwise difficult materials. Refractory metals and other hard materials can be machined with relative ease using the high temperatures and precision afforded by the spark erosion method. Wire EDM is used to carve out and design impressions in the workpiece material. This particular form of spark erosion is used in the die-making industry. The wire tool electrode is fed down to the work piece and can move along the X-Y-Z axes, allowing for the engraving or cutting of complicated shapes.

Although spark erosion is considered a removal process, it can also be used to add layers and coatings. Under sparking conditions, an anode steel electrode in the presence of a hydrocarbon dielectric will build a layer rich in carbon. This carbon-rich layer is known to increase the corrosion resistance of the base material. Similarly, titanium electrodes in a water dielectric develop an oxide layer. This process has been used to color titanium since the interference of light in the oxide film is responsible for the color of the titanium. A desired color can be achieved by controlling the thickness of the oxide layer.

The powder and particle industry also rely on spark erosion technology. The current intensity, current pulse length, current frequency, and electrode rotation speed can

be optimized to achieve of a desired size and size distribution. The process has been used to produce microspheres of metals, alloys, and compounds of a wide range of materials with particle sizes from several nanometers to several micrometers [22]. Processes that feature a rapidly rotating electrode are referred to as rotating electrode processes (REP) rather than spark erosion process. Although many spark erosion electrodes rotate, the method is distinguished from REP by the frequency of rotation (60 rpm vs. 10,000 rpm). REP is able to achieve much smaller particle sizes than non-rotating spark erosion methods because of the greater centrifugal force on the molten debris. The rapid rotation of the electrodes flings spherical debris from the gap but creates an elongated tail on the molten material. [23]. This tail eventually breaks from the primary debris particle and forms a smaller secondary particle.

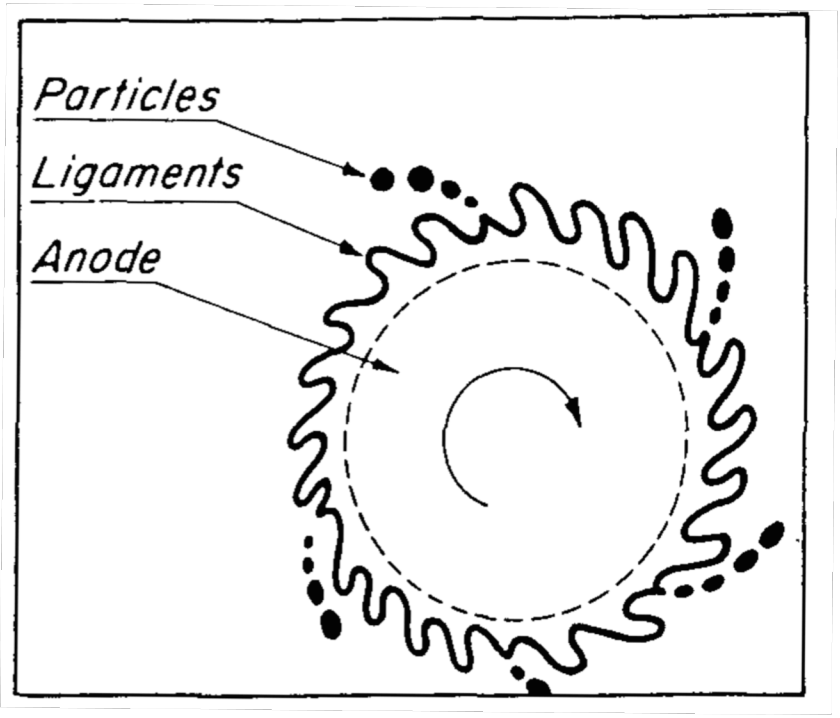

Figure 3.1: Shows how the molten debris flung from the rotating electrode can form a tail under high centrifugal forces. This tail will collapse into smaller debris spheres. [23]

Spark erosion can also be used to fabricate reacted particles. This is achieved by a reaction between the molten debris and the dielectric. The composition of particle and even the microstructure of the particle can be influenced by carrying the dielectric. It has been shown that kerosene and other hydrocarbon-based dielectrics form carbide phases in the reacted particles. Similarly, when water or deionized water is used as the dielectric, it is possible to produce oxide particles. To prevent the formation of reacted particles, an inert gas may be used as the dielectric.

3.2 Spark Erosion: Explanation and Underlying Principles

Both EDM and spark erosion refer to machining processes in which material is removed in response to a pulsed electric arc drawn across a pair of electrodes. One electrode is referred to as the tool electrode while the other is called the workpiece. A gap between the electrodes is filled with a dielectric, an insulating medium of gas or fluid. The dielectric aids in preventing electrolysis effects on the electrodes during the EDM process and is also responsible for the stability of the sparking behavior. Following the flow of current between electrodes, an electric discharge is initiated as the high voltage overcomes the dielectric breakdown strength of the gap. When the dielectric breakdown of the gap occurs, the gap transitions from an insulator to a conductor. This transition is characterized by the formation of a plasma channel, which is an ionized highly conductive gas with extremely high temperature. If the electrodes are not perfectly smoothed, the plasma channel tends to form at the nearest points between the electrodes. Following the formation of the plasma channel, an electric arc flows across the electrodes following the path of the plasma channel [19]. Plasma temperatures have been measured using spectroscopic analysis and were found to reach 6000-7000K [24-27]. Thus, the

electrode surface temperature rises well above its melting and even boiling point. The resulting molten material at the location of the arc is expelled from the gap. The molten debris material forms a sphere due to surface tension and solidifies as a result of the rapid cooling caused by the presence of a dielectric. When the flow of current is ended, the temperature of the plasma and the electrode surfaces rapidly drop. Hashimoto et al. found that the plasma temperature drops to below 5000K within 5μs after the discharge current is stopped [26]. This results in a recombination of ions and electrons in the gap and the recovery of the breakdown strength of dielectric.

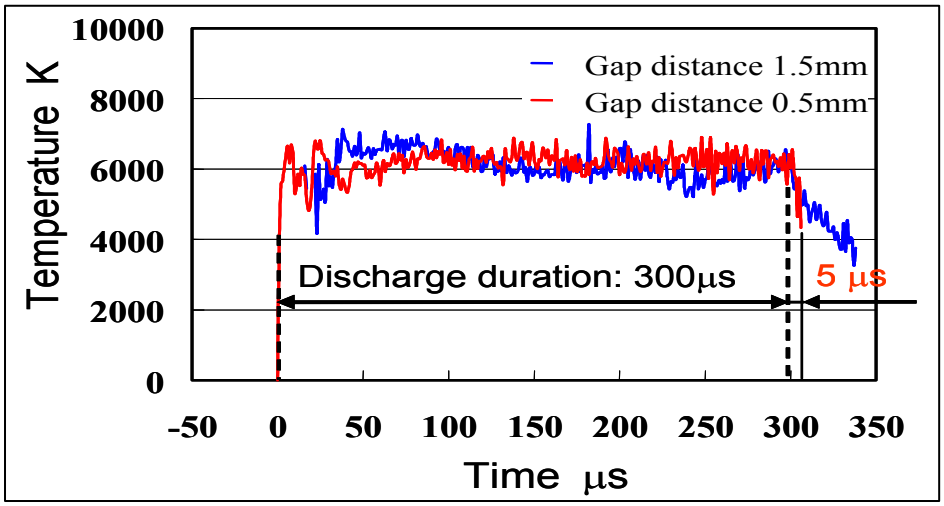

Figure 3.2: Plasma temperature at gap center during and after discharge as measured by spectroscopy [26]

Adequate timing between the applied current pulses insures that the dielectric has sufficient time to recover its breakdown strength. Hashimoto determined that applying the current before 5μs resulted in immediate ignition because the dielectric strength was not fully regained [26]. Thus, the frequency of the applied current used in EDM and spark erosion controls not only the frequency of the electric discharges, but also the stability of the process.

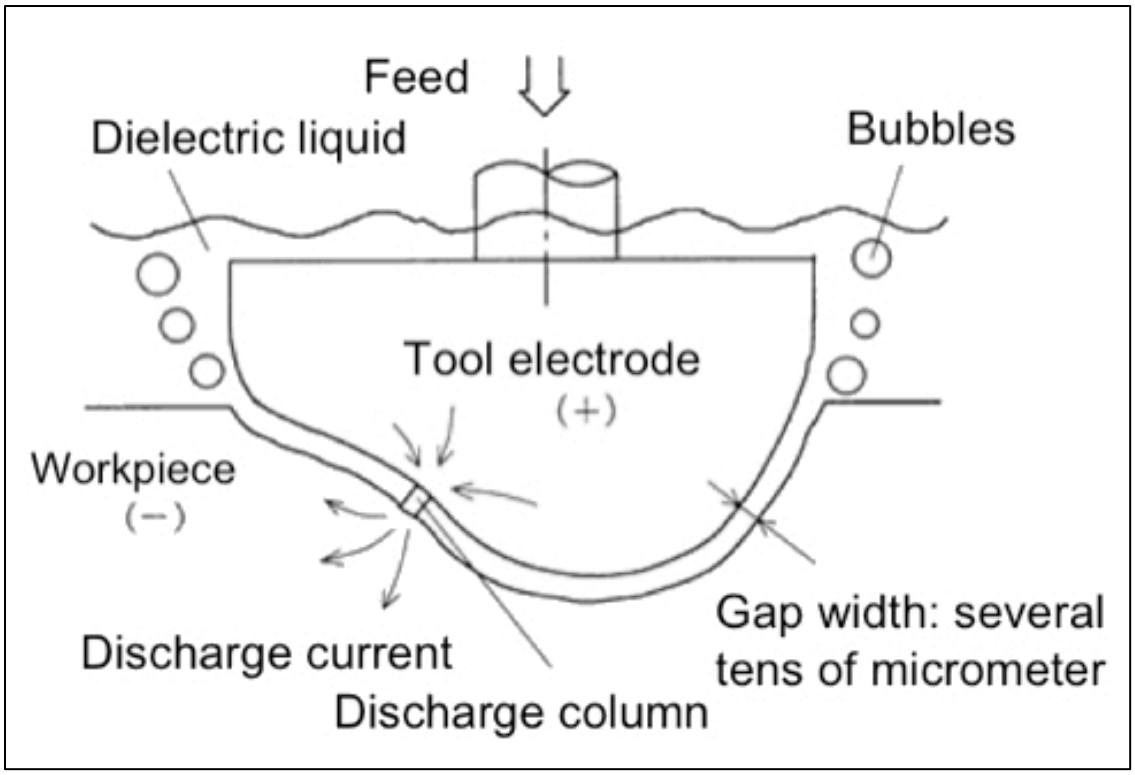

Figure 3.3: Example of Electric Discharge Machine. The tool electrode has a complex form in order to erode the workpiece into a desired shape. As the workpiece is eroded, the tool electrode is fed downward to maintain a constant gap width. [19]

3.2.1 Material Removal in the Gap

Several mechanisms may be used to aid in removal of molten material from the gap. This is required to prevent the buildup of debris on the surface of the electrodes. Additionally, the presence of debris in the gap results in unpredictable sparking behavior. In high-frequency rotating electrode processes, centrifugal forces are responsible for debris expulsion. A constant flow of the dielectric fluid or gas through the gap also aids in debris removal. This can be provided in cases where the dielectric requires filtration over the course of the experiment. In instances where the dielectric does not circulate during the experiment, the tool electrode may be intermittently raised and lowered in a pulsing-fashion in order to flush debris from the gap. The current research included in this thesis utilizes a pulsing electrode as a means of debris removal.

Ekman, et al. describes yet another mechanism of debris removal that occurs naturally due to the sparking process [28]. As the dielectric fluid is evaporated, molecules are dissociated and atoms are ionized, which result in the formation and rapid expansion of a gas bubble within the gap. The expansion of the bubble can occur at rates of tens of m/s [24, 28]. The rapidly expanding bubble blows out the particulate debris beyond the width of the gap. Thus, the high pressure and velocity field in the bubble provide a means of flushing and serve as the dynamics of debris removal.

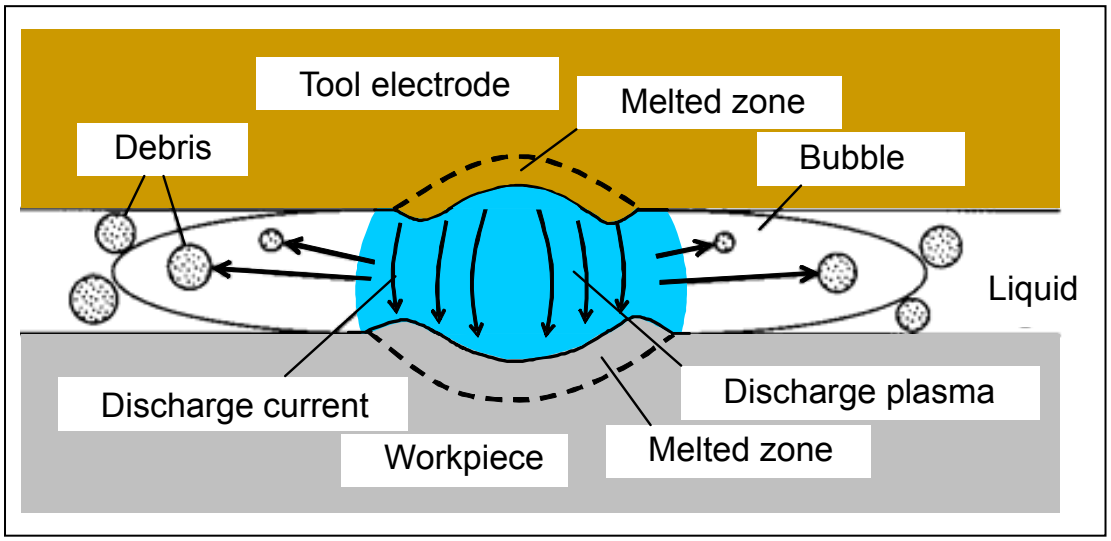

Figure 3.4: Discharge phenomena in the gap and the expulsion of debris [19]

3.2.2 Electrode Polarity

The energy dissipated to the anode is generally greater than that to the cathode [29]. Xia et al. found that when copper was used for both the anode and cathode, the energy distributed to the anode is about 40% and 25% to the cathode. The remaining energy contributes to the dissociation and ionization of molecules in the gap. Although energy preference due to polarity contributes to material removal, it is not the only mechanism responsible.

3.2.3 Thermophysical Properties of the Electrodes

The thermophysical properties of the electrode material are responsible for the temperature profile across the electrodes and ultimately for the material removal conditions. Saito et al. found that although the melting point of copper is much lower than that of steel (1355K vs. 1800K), the melted zone of copper is considerably smaller than that of steel due to its higher thermal diffusivity (1.1×10^{-4} m^2/s vs. $2.0 \times 10^{-5} m^2/s$) [30]. In the case of copper, the melted zone may even resolidify during the discharge duration. Because the surface temperature drops rapidly in copper, the time needed for the plasma to be extinguished is short. This leads to stable machining and explains why copper is a popular choice for the tool electrode in many spark erosion applications. Chemical Vapor Deposited (CVD)-carbon and electrically conductive CVD-diamond have also been used as tool electrodes and due to their high thermal diffusivities performed with virtually no wear of the tool electrode. Conductive materials are easily machined but it is now recognized that non-conducting materials, like ceramics, can also be machined if they are first coated with an electrically conductive layer.

3.2.4 Dielectric

The dielectric serves the purpose of insulating the gap until the moment of dielectric breakdown, at which point the plasma column across the gap assumes the role of an electrical conductor. The dielectric may be a gas or a liquid. The most commonly used gas is air, in a process referred to as dry EDM. This avoids the issue of filtration but the majority of removed material is reattached to the workpiece surface in the absence of a dielectric. Without a dielectric, the debris will not solidify until it hits the surface of the tool electrode [31]. In the presence of a dielectric fluid, the debris particles decelerate when they penetrate the bubble wall. Then, the debris solidifies into a spherical shape as

a result of surface tension. Processes that focus on the ejected debris require liquid dielectrics to prevent the molten debris from reattaching to the electrode surface.

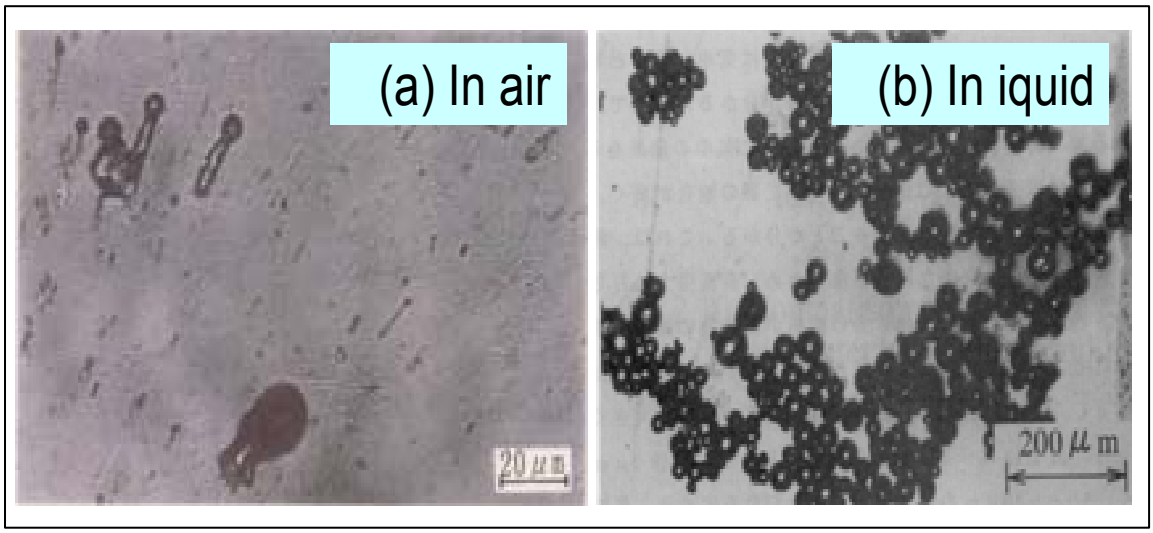

Figure 3.5: The variation in debris shape between air and liquid dielectric [31]

Deionized water or hydrocarbons may be used as liquid dielectrics. Each uniquely influences the behavior within the gap and can be used to produce reacted particles. However, safety must also be a consideration when selecting a dielectric. The use of a hydrocarbon, like kerosene, as a dielectric requires proper ventilation because hydrocarbons decompose and release harmful vapors like carbon monoxide and methane during the erosion process [33]. Hydrocarbon-based dielectrics tend to yield carbide particles, while deionized water can be used to form oxide particulates [22, 42]. Cabanillas also found that the microstructure of spark eroded particles varied between dielectric [50]. Iron particles produced in deionized water were predominately hollow. This was observed far less when iron particles were produced in kerosene. A subsequent effort using Uranium-Molybdenum electrodes to produce particles in water also yielded similar results. The observed voids were not smooth but rather featured large inclusions as shown in figure 3.6 [42]. An EDS analysis also indicated that the center of solid

spheres in the distribution varied greatly from the outer rim of the spheres. In fact, the composition of the inner body was highly non-uniform across the center of a single particle. XRD analysis of the Cabanillas U-Mo spheres revealed that the majority of particles were UO_2. Density measurements showed the particles had a mean density of 9.86 g/cm^3. Because the density of U-Mo phases range between 17 and 19 g/cm^3, Cabanillas reasoned that the measured density was further proof that the particles were UO_2. However, the density measurement also reiterates the porous and even hollow nature of particles produced when using deionized water as a dielectric.

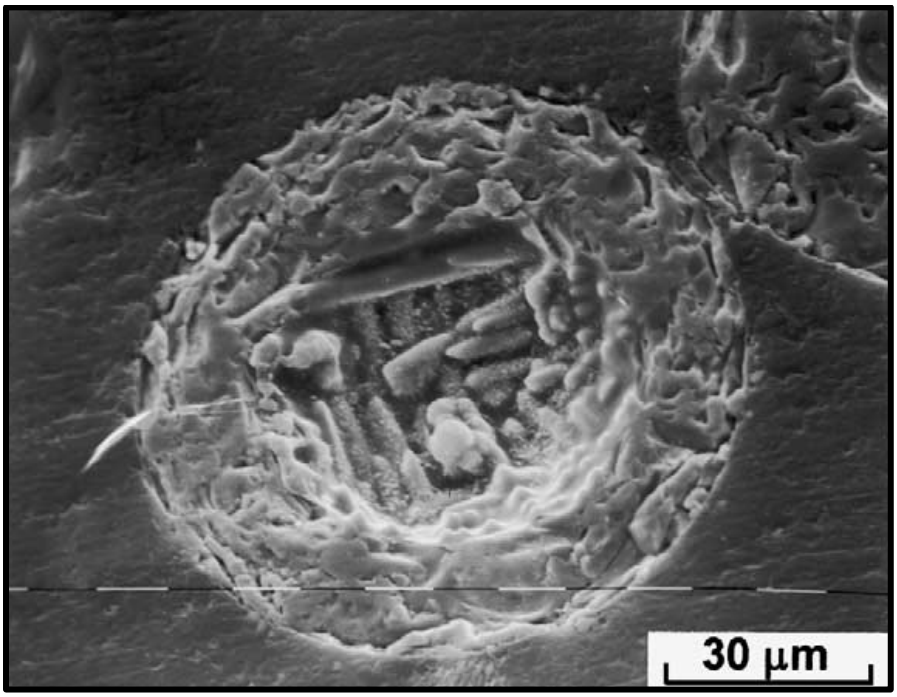

Figure 3.6: Image taken from Cabanillas [42]. Reveals oxidized internal structure of U-Mo particle produced in deionized water. [42]

The material removal rate may also be influenced by the choice of dielectric. Jilani, et al. compared the material removal rates for tap water and deionized water [34]. The highest machining rates were observed for tap water. Similarly, Jeshwani et al.

compared the material removal rates in kerosene and distilled water dielectrics. He noticed higher material removal rates in distilled water [35]. However, this study focused on workpiece machining rather than particle production. In terms of particle yield, Vasudevamurthy found that yield actually increased in kerosene rather than deionized water.

3.2.5 Gap Width

The gap distance between electrodes should be held constant for erosion processes focused on particle production. Variations in the gap distance change the rate at which the dielectric strength of the gap is recovered. If the gap is not held constant for successive discharges, the frequency of discharges can become erratic or the system may even short circuit. Thus, as material is removed from the workpiece, it is necessary to feed the tool electrode closer to the workpiece. Manually, this would be problematic because the gap distance is often maintained at a value less than 100 microns. Instead, servo feed control systems are utilized which automatically control the tool electrode feed rate based on a measured resistivity across the gap. When the measured average gap voltage is higher than the servo reference voltage, the feed rate increases. Conversely, if the average gap is lower than the servo reference voltage, the electrode is retracted or the feed rate is decreased [19]. By maintaining a constant working gap, servo feed control systems provide stable conditions, prevent short circuits, and increase the efficiency of the machining process.

3.2.6 Debris Filtration and Removal from the Dielectric

The presence of material debris or fabricated particles in the dielectric impacts the performance of the system. Depending upon the application, the presence of debris may be beneficial. In the machining industry, it has been found that the addition of a fine

powder to the dielectric can improve the material removal process and even improve the surface characteristics of the machined workpiece. This hybrid material removal process is called Powder Mixed EDM (PMEDM) [36, 37]. Electrically conductive powders reduce the insulating strength of the dielectric, which improves the machining efficiency and material removal rate. Conductive powders have also been found to lower the surface roughness of the electrode when added to the dielectric [38]. Similarly, very fine powders have been used in finishing applications of EDM in order to produce mirror-like finishes. Frequently used powders include Silicon Carbide, Aluminum, Chromium, Copper, and even crushed glass [38-41]. The addition of powder may range from 4g/l to 40g/l. In either case, the presence of fine conductive particles in the dielectric actually increases the material removal rate and the overall efficiency of the process. This has an important consequence for particle production via spark erosion. If fabricated particles in a given experiment are allowed to remain in the dielectric and are not filtered during the experiment; they, themselves, may change gap conditions. Conductive particles produced during spark erosion will decrease the insulating strength of the dielectric. Because a decrease in the insulating strength of the dielectric is associated with an increase in the material removal rate, the performance of the system will change. This may affect particle production in one of two ways; it may increase the particle yield while maintaining particle size, or it could increase the size of particles produced. Thus, the particle yield as a function of experiment duration is investigated in this work in order to check for potential nonlinear production rates.

3.3 Spark Erosion for Particle Production: Parameters which Influence Particle Size

Spark erosion can be used to produce highly spherical particles ranging in size from a few nanometers to ~100 micrometers [4]. The size of fabricated particles is controlled by a combination of several experimental parameters: current intensity, current pulse length, current pulse width or frequency, choice of dielectric, and rotation frequency of the workpiece.

The applied current provides the energy for the spark. The spark is responsible for depositing thermal energy to the workpiece, which in turn melts the workpiece. Because the applied current contributes to the sparking energy, it is not surprising that higher intensity currents result in larger sized particles. Comparably, smaller sized particles are achieved by decreasing the intensity of the applied current. This relationship between current intensity and particle size has been observed throughout the literature [4, 19, 22, 42, 43, 44, 45]. A less obvious relationship is the impact of current intensity on the distribution of particle sizes. Carrey and Berkowitz determined that a reduction in current widens the size distribution of particles [4]. Although a small current produces smaller sized particles, it does not provide the narrow size distribution associated with large currents. Regardless of the current magnitude, a bimodal size distribution is common, assuming smaller particles are grouped together. This was first observed by Svedberg, who noted that particles produced using an oscillatory arc yielded a bimodal size distribution. He concluded that fine particles formed by the condensation of vaporized material, whereas larger particles resulted from the solidification of molten debris [44].

As stated above, the current amplitude provides the energy for the spark. However, the energy of the spark also depends upon the duration of the applied current [4]. The duration of the current pulse is referred to as the pulse length. This also impacts particle size because it relates to the spark duration. Berkowitz found that as the pulse length or current duration was decreased, the size distribution shifted rapidly toward smaller particles. He proposed that pulse duration governed the diffusion time for thermal energy to travel away from the spark zone. As the thermal energy travels away from the spark zone, more molten material is created. Thus, shorter pulses impeded the formation of molten material and thereby, resulted in smaller particles [22].

The time between current pulses is called the pulse width or pulse-off time. It can also be thought of as the frequency of the applied current. This parameter has been found to influence a number of particle characteristics. Vasudevamurthy determined that shorter current pulse widths (more frequent pulses) resulted in a narrower particle size distribution [43]. Carrey also found that pulse frequency influenced the yield of particles. A high frequency produced a high particle yield. This led Carry to suggest that the best recipe for producing a significant amount of small particles is a low current at a high pulse frequency [4].

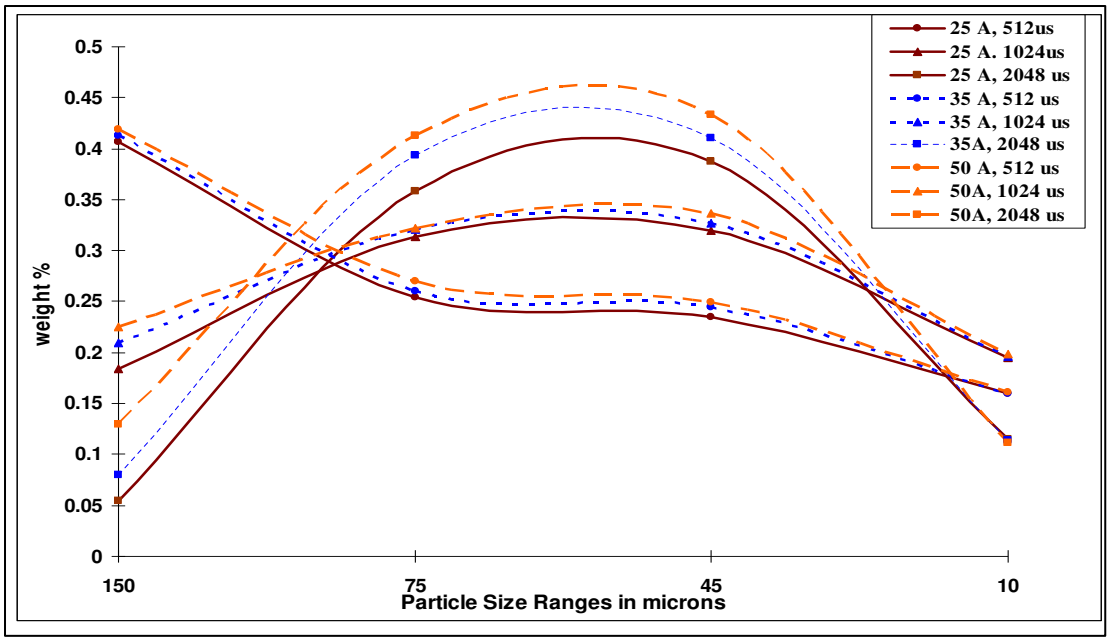

Figure 3.7: Size distribution of steel particles produced in a water dielectric. Data sets are a function of the applied current and the pulse width (frequency). Short pulse widths resulted in a narrower size distribution. [43]

Dielectrics can be selected to produce reacted or non-reacted particles. There is not a direct link in the research to suggest that the dielectric has an affect on particle size. However, it is reasonable to assume that in the case of reactions between the dielectric and particle, the fabricated particles will assume a new crystal structure and likewise new material properties, which will influence solidification and size. Thus, particles may be sized differently than a particle produced in a similar but non-reacting scenario. Variations in dielectrics have been shown to influence machining rate but this was observed in machining applications where the material removed was not nearly as important as the finished workpiece [34-35]. However, when Vasudevamurthy produced particles in Kerosene and water dielectrics he determined that the dielectric did influence the particle yield. Specifically, he found that the yield of particles was higher in kerosene than in water.

The rotation speed of the workpiece electrode can also have an influence on particle size. However, devices that offer such capabilities are referred to as REP rather than spark erosion. Nevertheless, it is important to discuss this effect since it contributes to particle size. In spark erosion, it is common to rotate the workpiece to encourage debris is flushed from the gap. The rotation applied in such cases is approximately 60 rpm [43]. As the angular rotation frequency of the electrode is increased, the centrifugal forces, which are felt by the molten debris, increase as well. When the centrifugal forces exceed the surface tension of the molten debris, the debris can separate into two or more smaller spheres [23]. Champagne et al. found that the size distribution of particles was influenced by the angular velocity of the electrode, the diameter of the rotating electrode, and the surface tension, density, and melting rate of the molten material [45]. The angular velocity of the electrode was inversely proportional to the median diameter of particles produced. In contrast to most spark erosion devices used for particle production, the rotating electrode device used by Champagne operated with a rotation speed between 6,000-15,000 rpm. Angers noted that the upper limit for angular velocity was 20,000 rpm [46]. Rotation speeds above this value resulted in mechanical problems due to an inability to balance the system [46].

It can be concluded that in order to produce a high yield of small particles within a narrow size distribution, a high frequency, low intensity current with relatively short pulse duration should be selected. Additionally, if it is possible to rotate the workpiece electrode at a high angular velocity, even smaller particles may be achieved.

CHAPTER 4

FABRICATION OF SURROGATE FUEL PARTICLES

4.1 EXPERIMENT CONDITIONS:

The spark erosion device used in this research was custom-built by CT Electromechanica of Argentina. The device consists of a rotating part and a stationary part. The upper rotating part includes a fixed speed servomotor (60 rpm) and workpiece holder. A microprocessor-based servomechanism controls both the work piece electrode rotation and axial movement. The work piece electrode can be repeatedly withdrawn from the gap (pulsed in an upward and downward motion) in order to flush debris particles from the gap. A catchment tank and a tool electrode holder comprise the stationary part of the device. The power to the system is supplied by a solid-state power unit capable of delivering square wave AC currents in the range between 200 mA and 50 A. The device can provide variable current pulses and variable pulse widths between 2 μs and 2048 μs. The positive and negative terminals can be alternated in order to produce the desired polarity across the electrodes. This research utilized direct polarity as recommended by the device's user manual (negative terminal connected to the steel workpiece electrode positive terminal to the copper tool electrode). As discussed in chapter 3, varying the arc intensity, pulse length, and pulse width make it is possible to produce a wide range of particle sizes and distributions.

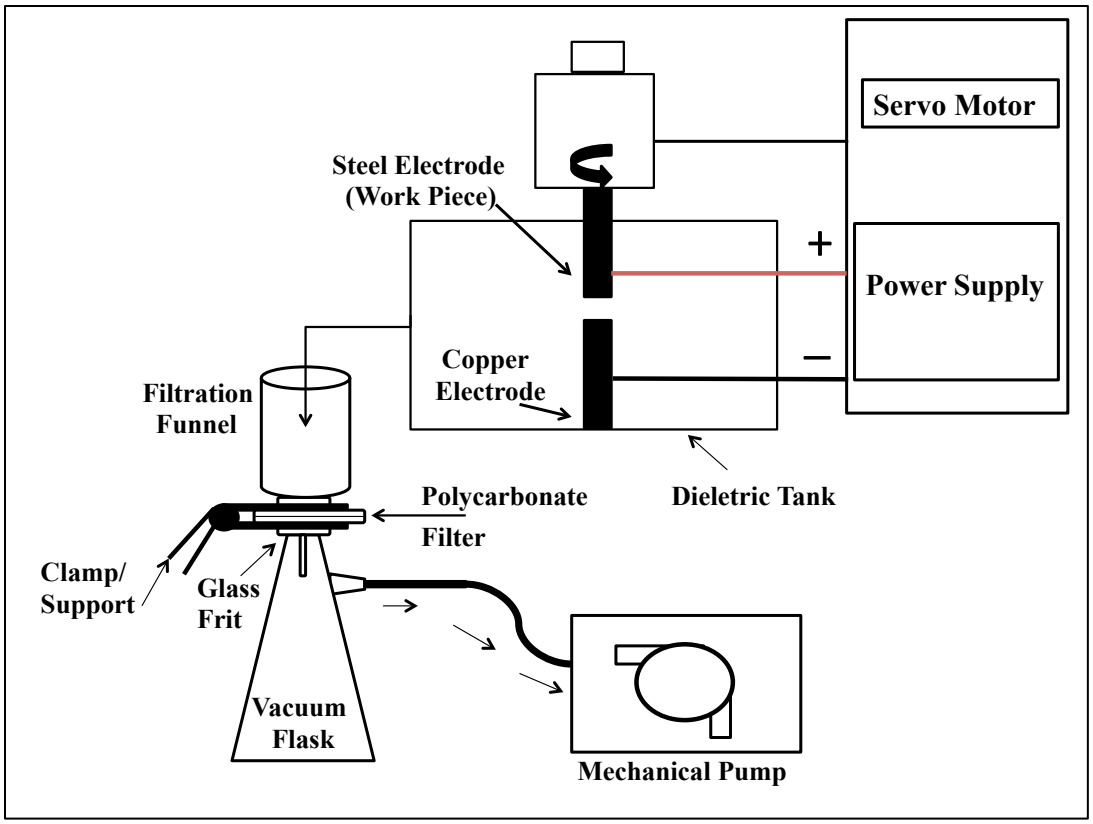

Figure 4.1 Experimental setup including filtration system

The literature review in the preceding chapter revealed that in order to produce a high yield of small particles within a narrow size distribution, a high frequency, low intensity arc with relatively short pulse duration should be selected. The experimental parameters were informed by the results reported by Berkowitz, Carrey, Cabanillas, and Vasudevamurthy [4, 22, 42-43, 47]. The results from Cabanillas and Vasudevamurthy were given the most consideration because the device used in the current research was used in both their research efforts.

In order to maintain a high sparking frequency, 64 μs was selected as the pulse width. When Vasudevamurthy used this value, he produced a large yield of particles [43]. Additionally, when Cabanillas used 64 μs in his research he yielded a bimodal distribution of particles, with the majority of particles on the order of 10 μm [42].

A short pulse length was selected since it impacts the diffusion time of the material melt, and thus the particle size. For a fixed current, Vasudevamurthy reported the yield of small particles increased when the pulse length was shortened. Therefore, the smallest value used by Vasudevamurthy, 512 μs, was chosen as a starting parameter for the current research.

The relationship between arc intensity and particle size is well documented in the literature; in order to produce small particles, it is necessary to use small arc intensities. Although the spark erosion device used in this research could generate arc currents as low as 200 mA, extremely small currents were deemed unfavorable because they were associated with a wider size distribution [43]. When Cabanillas generated 10-micron particles, he used 25 A as the arcing current. Therefore, three arc intensities (10 A, 16 A, 25 A) were chosen to determine the optimal arcing current required for the fabrication of 10-micron particles.

The gap width conditions are often generalized in the literature. Kuneida recommended that the gap be maintained between 10 μm and 100 μm for optimal arcing conditions [19]. In order to prevent particles from remaining in the gap or forming agglomerates, a larger gap was favored and the value of 100 μm was chosen. In order to promote debris removal from the gap, it is customary to rotate the workpiece, withdraw the workpiece, circulate the dielectric through the gap, or a combination of the three. Based on the particle filtration system chosen (discussed in section 4.3), continual circulation of the dielectric was not desired. When the dielectric was circulated through an inline filter, it was found that a significant quantity of particles was lost to the tubing. Therefore, the dielectric was not circulated or filtered during the experiment. Instead, the

rotation of the workpiece was fixed at 60 rpm to encourage flushing of the gap. Additionally, a "washing" mechanism was employed in which the workpiece was axially pulsed during the experiment. The CT Electromechanica user manual referred to the motion as a "washing" mode because it promoted the flushing of debris from the gap. The frequency of the upward and downward motion could be adjusted to maximize the time when the electrodes were closest. The gap was 100 µm approximately ¾ of the time. The other quarter of the time was spent raising and lowering the electrode by approximately a millimeter. The repeated motion of the steel workpiece encouraged the flushing of debris particles generated during sparking and maintained stable arcing conditions in the gap. Table 4.1 provides parameters from literature used in the selection of experimental conditions for this research.

Table 4.1: Experimental parameters used in particle production research and resulting particle sizes

Experiment	Particle Size	Dielectric	Current	Notes
Berkowitz, 1987--Iron alloy	75 µm	kerosene, silicone oil, dodecane	1-5 A	Frequency 10-40 kHz; 10-20 V; gap is 50 µm
Carey, 2004--Nickel	1-20 nm	deionized H2O, dodecane, kerosene, liquid Nitrogen	---- Varied Voltage	Pulse length 1-2000 µs; 10-20 V; gap is 50 µm
Vasudevamurthy, 2007--304 SS	<45 µm, 45-75 µm, 75-150 µm, >150 µm	deionized H2O	25, 35, 50 A	Pulse length 512; 1024,2048 µs; Pulse width 64 µs; 80 V
Cabanillas, 2004--U-Mo	bimodal (10 and 70 µm) ----Most are 10 µm	deionized H2O	25 A	Pulse length 2048 µs; Pulse width 64 µs; 80 V
Cabanillas, 2007--Alpha-Iron	bimodal-micron (44-53 µm) and nano (5-10 nm)	kerosene	25 A	Pulse length 3,072 µs; Pulse width 25,589 µs; 80 V

In summary, for the research contained herein, the pulse length (duration of the pulse) was maintained at 512 µs and the pulse width (pulse-off) at 64 µs for all runs. Three current intensities (10 A, 16 A, 25 A) were chosen to examine the relationship between arc intensity and particle size. The gap width was held constant at 100 µm

during sparking and the workpiece was withdrawn and lowered every three seconds in order to flush the gap between sparks. To investigate the fabrication rate as a function of experiment duration, an additional set of experiments were conducted. The experimental conditions were the same as those described above, except current was held constant at 16 A. Experimental yield was examined for durations between 15 minutes and 3 hours to determine if the added presence of particles in the dielectric affected sparking conditions, and as a result, increased particle production rates.

4.2 Experimental Procedures

Prior to each experiment, the catchment tank and filtration tubing were rinsed. Approximately 4600 mL of deionized water was used for each experiment in order to fully submerge the copper electrode and partially submerge the steel electrode. The water level is shown in figure 4.2.

The steel electrode was cut to 5 cm and the copper electrode was cut to 3 cm. Additionally, the copper and steel electrodes were ground and polished prior to each experiment in order to provide identical starting conditions. It was extremely important that the surface of each electrode was perfectly flat prior to each experiment because sparks formed preferentially between points of closest contact. If the electrode surfaces were not level at the outset of the experiment, the steel electrode wear was uneven and resulted in irregular sparking and reduced particle yield. Images of the electrodes before and after an experiment are shown in figures 4.4 and 4.5.

Figure 4.2: Electric discharge setup. The steel work-piece rotates while the copper tool electrode is anchored to tank base.

In order for the servomechanism to maintain the desired gap width during the experiment, the electrodes positions were first "zeroed" to provide a reference point. This was accomplished by manually moving the workpiece holder downward until the two electrodes made contact. This position was then recorded in the control system to provide a reference point. The steel workpiece was then raised so that there was a 100-μm gap between the two electrodes.

After the workpiece electrode motion was initiated, the desired current was applied to the system. The duration of each experimental run was approximately 2 hours. However, this value was increased to 3 hours for the 10 A experiments because it was determined that additional time was needed to yield of sufficient amount of particles for characterization. When the run was completed, the power was turned off and the dielectric and suspended particles were filtered from the catchment tank.

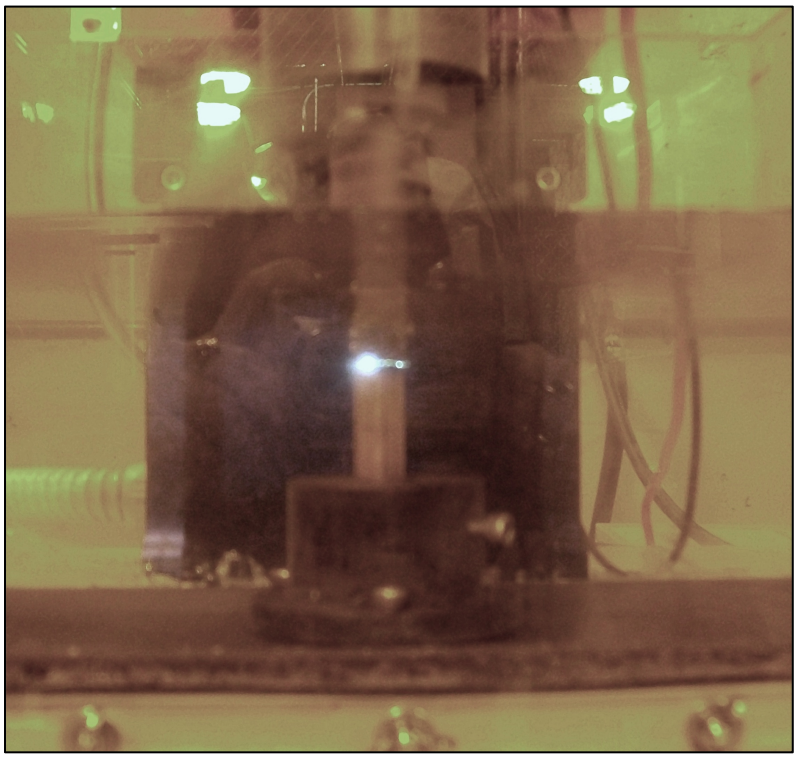

Figure 4.3: A spark is shown between the steel workpiece and copper tool electrode.

Following each experiment, the electrodes were removed from their holders and washed in the dielectric tank water in order to retain any particles stuck to the electrodes. As can be seen in figure 4.4, the copper tool electrode showed little wear to its surface. Instead, the surface appeared to have a very thin deposit on its surface due to the deposition of melted debris from the steel workpiece. The deposit was removed easily

during the electrode polishing process. The overall smooth surface of the copper electrode indicates that there was no material removed from its surface. However, the steel electrode revealed numerous craters along its surface. These craters or pores reveal the locations of the sparks. In fact, upon visual inspection, the pore sizes depended upon the current used in the experiment. This can be explained by the fact that current intensity determines particle size and the spark energy influences the amount of material melted during arcing. As the molten material is expelled and forms a particle, it leaves a crater that is indicative of particle size.

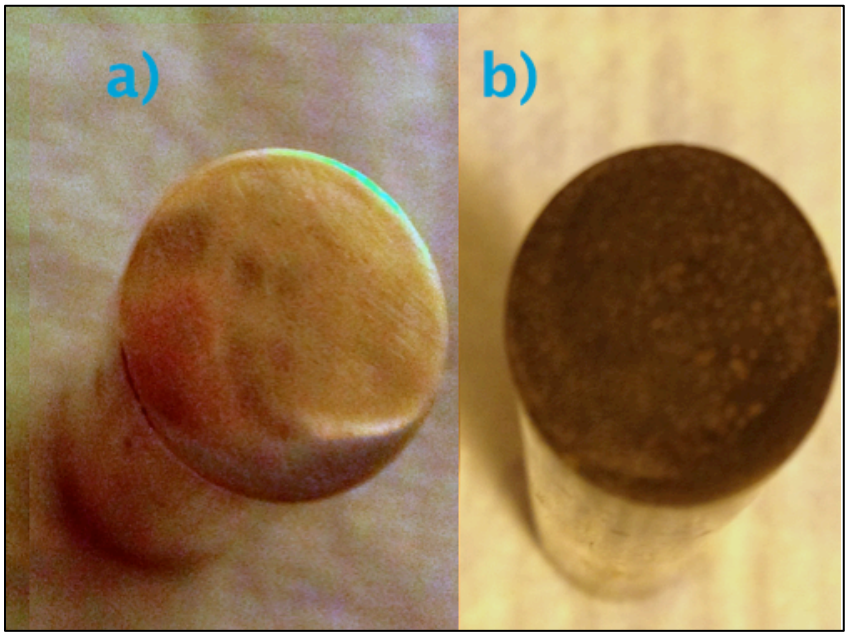

Figure 4.4: Copper electrodes. a) Polished electrode prior to Experiment b) Surface of copper electrode after experiment; the electrode does not reveal any material loss.

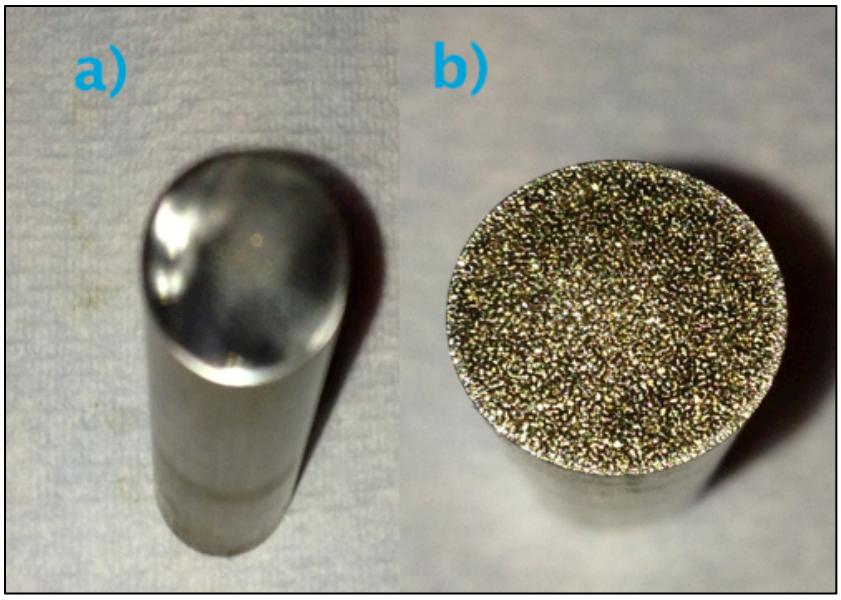

Figure 4.5: Steel Electrode a) Polished electrode prior to experiment b) Surface of the steel electrode after experiment reveals numerous micron-sized craters.

4.3 Particle Filtration

One of the greatest challenges presented by this research was the filtration and separation of the 10-micron particles from the dielectric. Vasudevamurthy used an inline peristaltic pump and thread filter and continuously filtered the dielectric fluid during operation [43]. This technique was the first approach used for particle filtration. A peristaltic pump on the outlet of the filter drove the water from the dielectric tank to the filter and back to the base of the tank where the water flowed up around the copper electrode. After the first several attempts, the thread filter system was deemed ineffective because the thread filter maintained all fabricated particles and did not allow for particle removal.

The next motion was to swap filters for a smaller, serviceable inline filter from Industrial Specialties Inc. This filter was constructed from porous polypropylene and claimed particle retention down to 1 micron. The motivation for this filtration approach

was guided by the use of multiple inline filters as reported by Cabanillas [42]. However, this filter also retained too many of the fabricated particles. Additionally, utilizing a continuous filtration approached required an exorbitant amount of time to ensure the majority of particles were filter from the tank. Thus, the method of inline filtration was deemed impractical.

Next, a decanting system was constructed consisting of a funnel, flask, and drain connected to the base of the tank. The filtration was performed at the conclusion of the experiment. A piece of filter paper was inserted into the funnel. The flow rate of the coarse grain paper was too slow driven simply by gravity. Additionally, the coarse grain filter paper retained too many of the particles.

The next particle removal technique used was evaporation of the dielectric tank water at the end of each experiment. The evaporation method appeared promising because it eliminated the issue of liquid waste generated during spark erosion. Tank water was transferred to a beaker and heated over a hotplate. This worked well because it eliminated particle loss. However, this process was slow, evaporating at a rate of approximately of 2.6 ml/min. Additionally, even more deterring, was the fact that it was difficult to remove all particles from the beaker post evaporation.

The final idea for particle filtration was motivated by the technique documented by S.B. Slade et al. [48]. Slade employed multiple vacuum filtrations in order to separate particles within narrow size distributions. This method generates a large quantity of liquid waste, which would become problematic if used for production of nuclear materials. However, with a series of filtrations it may be possible to reuse the tank water and reduce the quantity of radioactive liquid waste. The filter used in the Slade research

was a Whatman Nuclepore© polycarbonate filter with separation capability of 3 μm. Whatman Inc. was contacted in order to determine the appropriate filter for this research. Samples were requested and using a smaller filtration system borrowed from another lab group, it was determined that the polycarbonate Nuclepore© filter was perfectly suited for the particle retrieval required by this research. The largest filter diameter available for the Nucleopore 3μm membrane filter is 90mm. This guided the purchase of an equally large filtration system from Kimball Chase, which supported a 90mm filter and 4000 mL of liquid. A large filter was desired to prevent particle buildup on the filter, which could slow the process of filtration. The filter was sandwiched between a glass frit support and the filtration funnel. A heavy-duty clamp was used to hold the filtration funnel and support in place, as well as maintain an airtight seal. Using vacuum tubing, the filtration unit was connected to a 0.75 HP mechanical pump in the laboratory.

Vacuum filtration proved to be the best option for particle retrieval. The catchment tank was directly drained into the filtration funnel. As the dielectric was drained, a wash bottle was used to rinse out the remaining particles in the tank. It should also be noted for future work that multi-filtration units capable of accepting 3 or 4 filters could be purchased to expedite filtration the process. Following filtration, the filter was easily removed from the glass frit and could be dried on a watch glass overnight. It was found that attempted removal of particles while they were still wet, led to unnecessary losses. When dried, the particles did not adhere to the filter and could easily be removed by carefully rolling the flexible filter into a tube and brushing remaining particles into a sample holder. The stages of the particle filtration process are shown in figure 4.7.

Collected particles were then weighed for yield analysis. Additional particle characterization consisted of Cu-Kα X-ray diffraction analysis, energy-dispersive spectroscopy, electron microscopy, gas pycnometry, and laser-light particle size analysis.

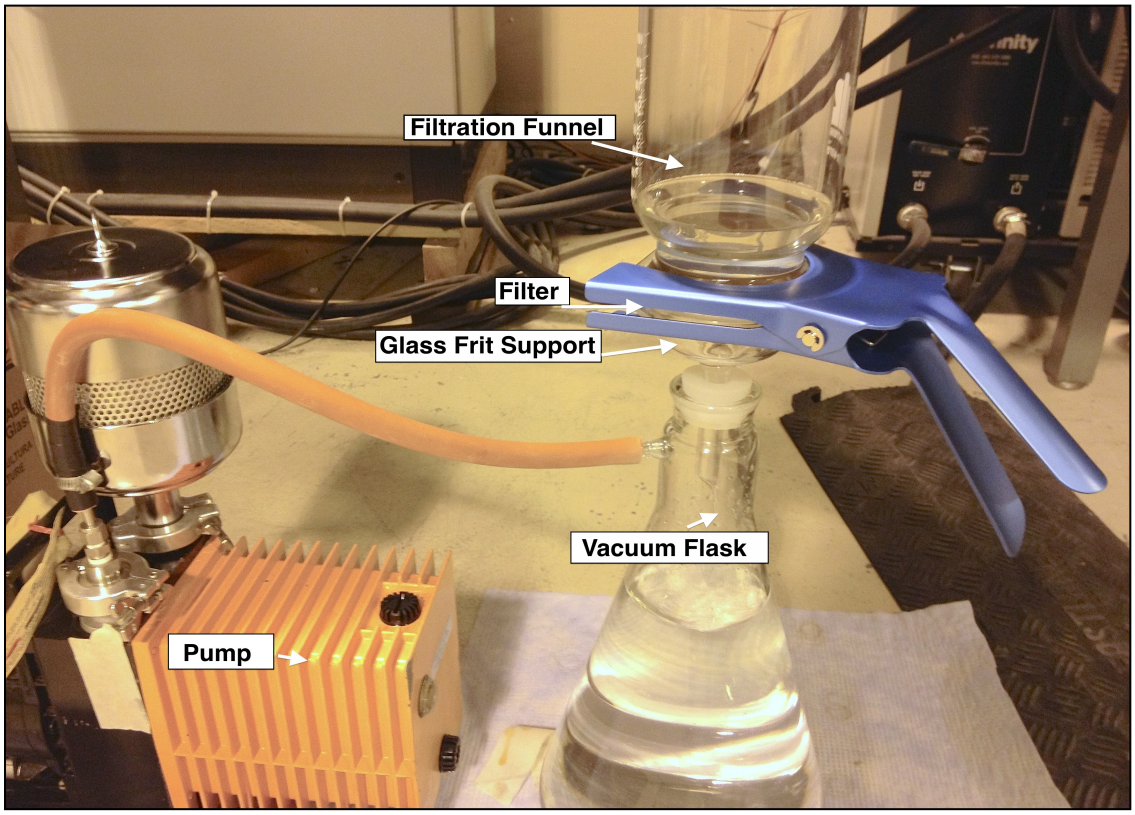

Figure 4.6: Vacuum filtration setup.

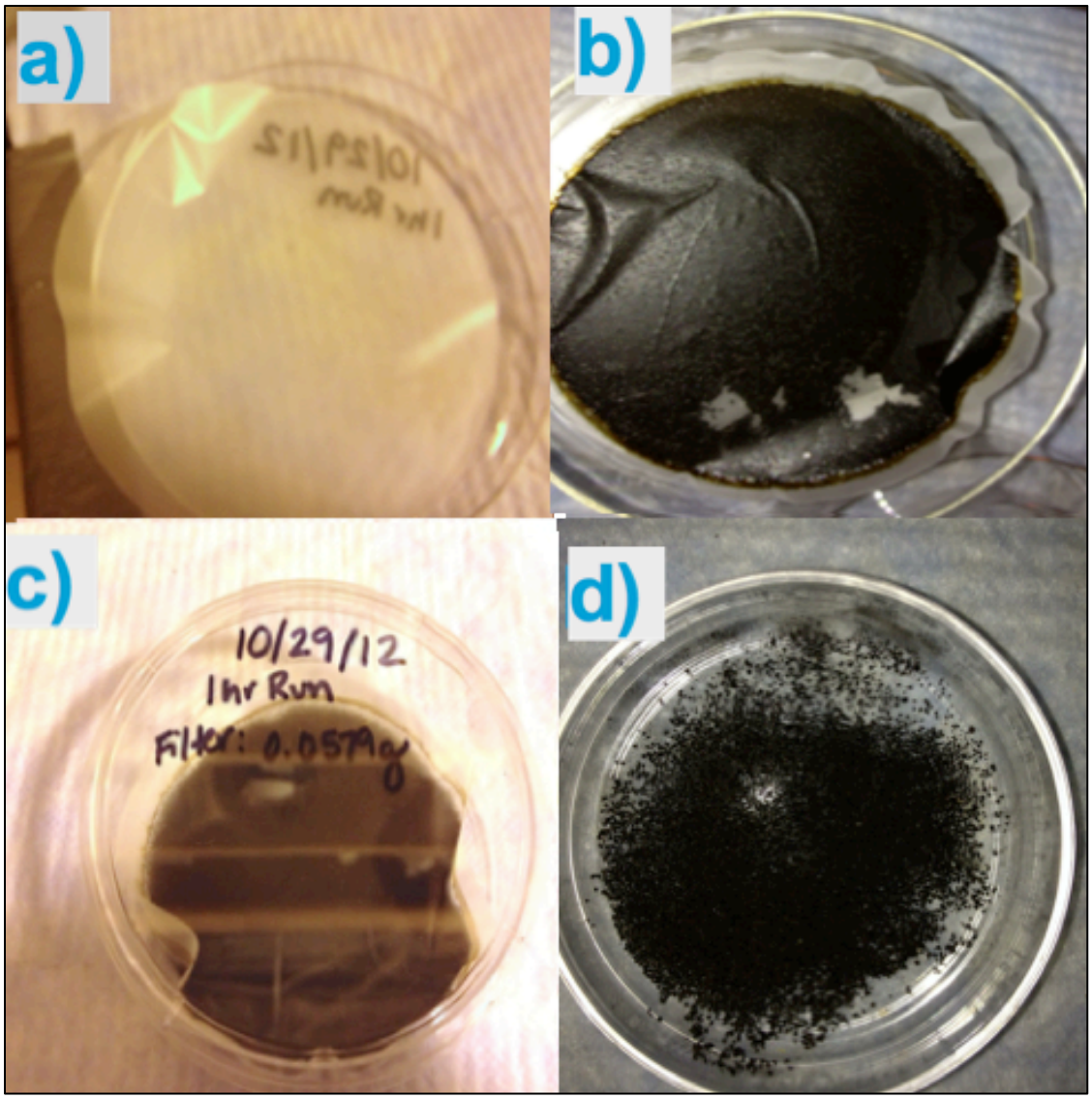

Figure 4.7: Polycarbonate filter a) Polycarbonate filter prior to filtration b) Wet particles are shown following filtration. c) Post filtration, particles have completely dried on the filter. d) Particles are removed from the flexible filter by a rolling motion stored in a sample dish.

CHAPTER 5

RESULTS AND CHARACTERIZATION

5.1 PARTICLE YIELD

The particle yield was desired for two reasons: to evaluate the efficiency of the system for scaled-up efforts and to determine if the presence of fabricated particles in the dielectric had any effect on particle production rate as is used in the Powder Mixed EDM industry (See section 3.2.6). To examine this, particle yield was recorded for a series of runs with durations between 15 minutes and 3 hours. To measure particle yield, the mass of the unused filter was compared to the mass of the filter + particles following filtration and drying.

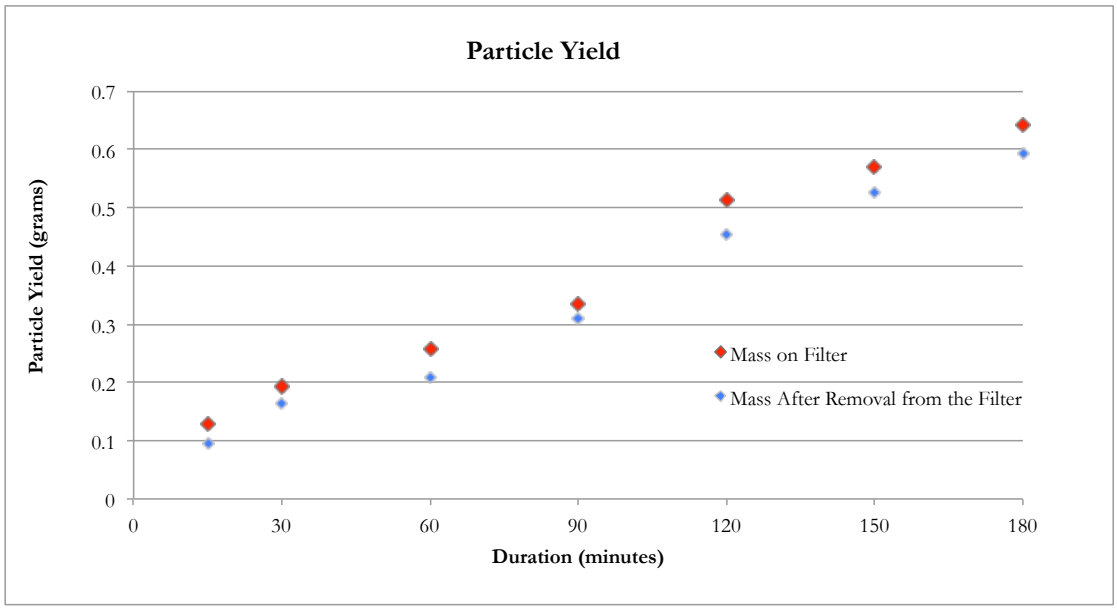

Figure 5.1: Particle yield as a function of experiment duration. (Experiment conditions were identical between tests, 16 A, 512 µs pulse length and 64 µs pulse width.)

The trend in particle yield as a function of experiment duration did not reveal conclusive evidence that particles in the system aid in the removal rates. Rather than observing an exponential or even polynomial increase, the particle yield appeared to increase linearly with experiment duration. It is possible that the phenomenon of increased material removal rate was not observed because the concentration of particles was lower than that used in the Powder Mixed EDM process. At any given time, the concentration stayed below 0.6 g per 4.6 L. Contrasted with the 4g/L utilized by the PMEDM industry, it is reasonable to assume that the concentrations were too low under the research conditions to observe any increased removal rates that may occur with the build up of conductive particles in the dielectric.

The particle yield could easily be increased in scaled-up efforts if a large number of particles were required. Electrodes with larger diameters would provide a larger sparking surface and thereby increase the rate at which particles are produced. Additionally, eliminating the wash mechanism used to pulse the workpiece in the gap would increase the amount of time available for sparking. This would most certainly increase the particle yield as a function of time. However, another flushing mechanism would need to be employed to ensure that debris in the gap was expelled between consecutive sparks.

5.2 Particle Losses

The system used to fabricate spark-eroded particles was evaluated in terms of its ability to produce particles with minimal losses. This is required in order to ensure the process is competitive and efficient. In the nuclear industry, material accountability also

dictates the feasibility of a process. Therefore, although particles in this research were fabricated from a surrogate material, it was important to identify opportunities for particle loss in the system in the event that the process is used for future work with radioactive materials.

It was desired to determine the amount of particles retained by the tank and tubing following each filtration. At the outset of the experimental runs, the tank was cleaned and fresh tubing installed. The mass of the tubing was recorded. A two-hour spark erosion experiment (16 A, 512 μs pulse length, 64 μs pulse width) was then run and the tank was filtered according to procedures. The tank was flushed with a wash bottle to aid in particle removal. This ensured that the number of particles retained represented a realistic amount given the typical experiment conditions and the overall objective to reduce particle loss.

Following filtration, a pre-weighed Kimwipe™ was used to remove particles from the tank. Another wipe was used to remove particles that adhered to the inner surface of the filtration funnel. The wipes were place on watch glasses, covered, and allowed to air dry over the next two days. When dry, the wipes were reweighed to determine the amount of particles collected by the Kimwipe™. Similarly, the pre-weighed tubing, which allowed the flow of liquid and particles from the catchment tank to the filter funnel, was allowed to dry and then reweighed. Mass gain was assumed to be indicative of the amount of particles trapped in the tubing during a typical experiment. Table 5.1 provides the quantity of particles retained by the catchment tank, filter funnel, and tubing for a 2 hour run.

Table 5.1: Mass of particles retained in system for a 2hr run conducted at 16 A.

	Mass of Particles Trapped
Tank	0.085 g
Filter Funnel	0.016 g
Tubing	0.012 g
Total	0.011 g

The average particle loss due to fabrication and filtration was approximately 0.11g. The greatest losses were due to particle retention in the catchment tank. When each filter was reweighed following particle removal, it was determined that particle loss due to retention in the filter was negligible. The actual process of removing of particles from the filter resulted in some losses; however it was not due to retention of particles in the filter, itself. The use of a smaller catchment tank for future experiments would reduce the surface area available for particles to adhere to and reduce particle losses to the tank. Additionally, a smaller tank would require a smaller volume of the dielectric in order to submerge the electrodes. As a result, a smaller tank would generate less liquid waste during fabrication and filtration.

5.3 Particle Size Analysis

Particle size analysis was accomplished using a Micrometrics Saturn Digisizer [49]. Laser light particle analysis utilizes light sensitive detectors arranged around the sample, which respond to the instantaneous amount of light scattered. Particles were first added to a dispersion medium contained in the instrument. An automated liquid sample-handling unit continually recirculated the fluid in order to properly disperse each sample. The Digisizer records a wide range of measurements using a high-resolution charge-coupled device (CCD). Additionally, the collimator lens that delivers the laser light to

the sample cell can be rotated to provide additional measurements. This signal intensity (the amount of light scattered at different positions) is proportional to the size of particles and the ability to collect a higher resolution scattering pattern, results in a higher resolution size distribution.

The technique of particle size analysis by light scattering is based on Mie Theory. Mie theory provides the light scattered by an individual particle as a function of the scattering pattern produced by spherical particles of a specific size. By using a least squares fit, the Digisizer software fits the measured light scattering pattern to a theoretical particle size distribution.

The particle dispersant must be chosen according to the density and size of particles to be analyzed. Large, dense particles require viscous dispersants. Water can be used as a dispersant but should be circulated for many hours prior to the experiment to ensure that bubbles have left the system. Methanol and other alcohols are used as a rinsing fluid to flush the system between measurements. Because the fabricated particles were easily dispersed in methanol, methanol was selected as both the dispersant and rinse liquid. This greatly simplified the analysis and ensured that bubbles were not introduced into the system.

Prior to each experiment a background test for the methanol solution was performed. When the system was fully clean and filled with methanol, the background curve was well defined. Following each rinse between analyses, another background was run to check for residual particles in the system. If the resolution of the background spectrum was reduced in comparison to the initial methanol background, the system was flushed and rinsed until both background spectrums agreed. Figure 5.2 shows the

difference between an acceptable background measurement and a non-acceptable background measurement. The red curve (Background B) was the initial background measured for the methanol dispersant at the outset of all size analyses.

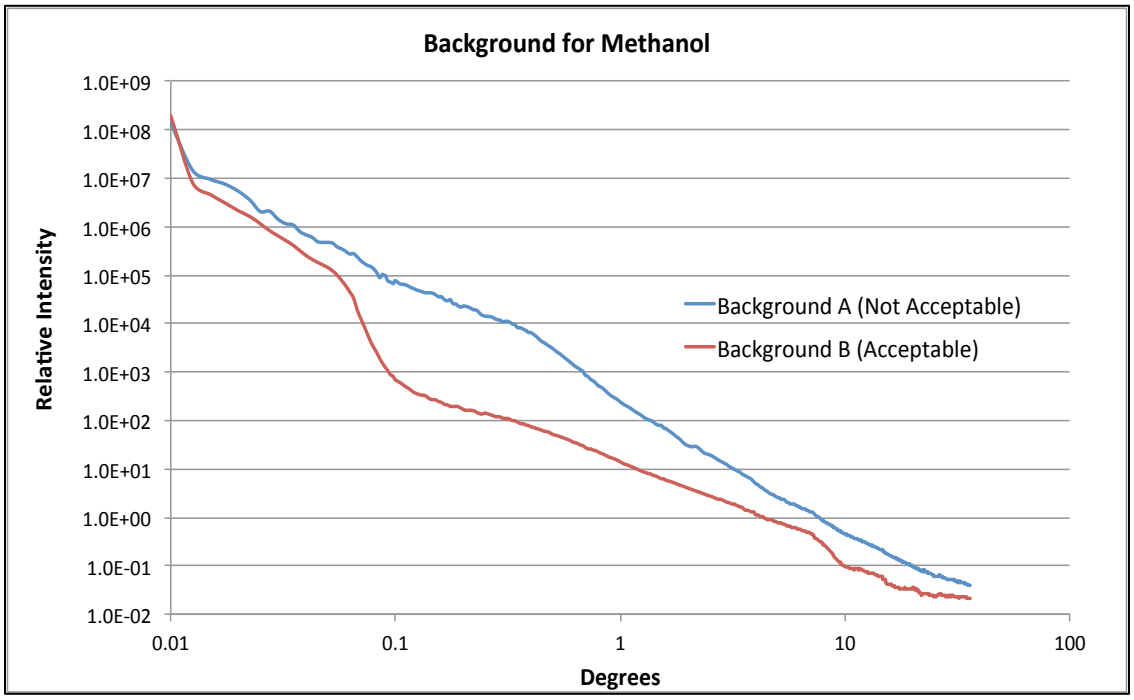

Figure 5.2: Background B shows an acceptable and well-defined background measurement. Background A has higher intensities and less detail. This indicates the presence of contaminants, which cause the light to scatter smoothly and continuously.

In addition to background testing, it is possible to reveal trace particulate matter in the system as a function of the present beam obscuration. The Digisizer indicates the obscurity of the dispersant as detected by the CCD and updates the value in real time. This reveals residual particles in the system following a rinse and allows for consistency between sample measurements. The recommended obscurity for a sample depends upon the expected size of the particles. For particles on the order of 1-100 micrometers, the recommended beam obscuration is 10%-20%. This required approximately 0.3 g -0.5 g of fabricated particles for each analysis.

Table 5.2: Sample concentration and beam obscuration for each sample

Sample Concentration			
Sample:	10 A	16 A	25 A
Sample Concentration (%):	0.00207	0.00387	0.00302
Obscuration (%) :	12.4	14.5	16.1

The analysis software for the Digisizer automatically subtracts the background intensity due to the methanol. Between each sample analysis, the system was rinsed twice with methanol to remove all particles. A background measurement was then performed to determine if any particles were retained in the system. If the background revealed that the system was free of contaminants, analysis with a different sample identity could be performed. Otherwise, the system was rinsed until both beam obscuration and background measurement indicated that the system was free of debris. Size analysis measurements were performed three times per sample (25 A, 16 A, and 10 A).

The Digisizer shows a high degree of reproducibility across the analyses performed for the 25 A sample. The histogram for the 25 A sample shows the largest frequency of particles occurring at a diameter of 12.46 μm for all three tests. The second largest peak is centered on a diameter of 8 μm. The size frequency then steadily decreases below 8 μm for all tests except test 3, in which a small yet pronounced peak is seen at 0.8 μm.

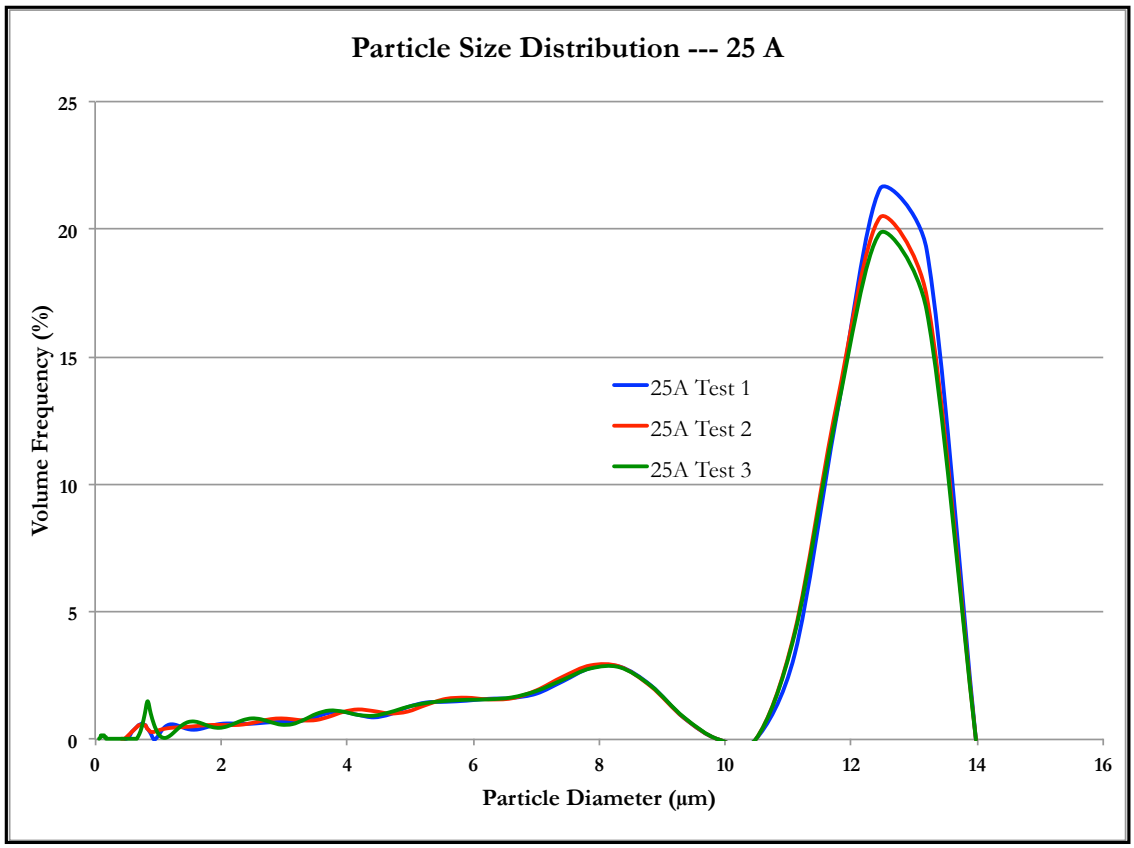

Figure 5.3: Results of 3 particle size measurements are graphed as a function of volume frequency for the 25 A sample. A summary of particle size data for each test is provided in table 5.3.

Table 5.3: Summary report for each 25 A sample Test

Volume Distribution --- 25 A Sample					
	Test 1	Test 2	Test 3	Cumulative Average	
	Diameter (µm)	Diameter (µm)	Diameter (µm)	Diameter (µm)	Std. Dev.
Mean	9.129	8.953	8.741	9.274	0.337
Median	11.70	11.50	11.37	11.523	0.136
Mode	12.46	12.46	12.46	12.46	0.000

The particle sample fabricated using a 16 A current followed a similar trend in size distribution as the 25 A sample, except values are shifted toward smaller diameters. As was observed in the 25A-sample, a single peak dominates the histogram of the 16 A-sample. This peak occurs at a value of 10.48 µm and is followed by a secondary peak

centered on 6.6 µm. Below 6.6 µm, there are several less pronounced peaks and then a final small peak over 0.7 µm.

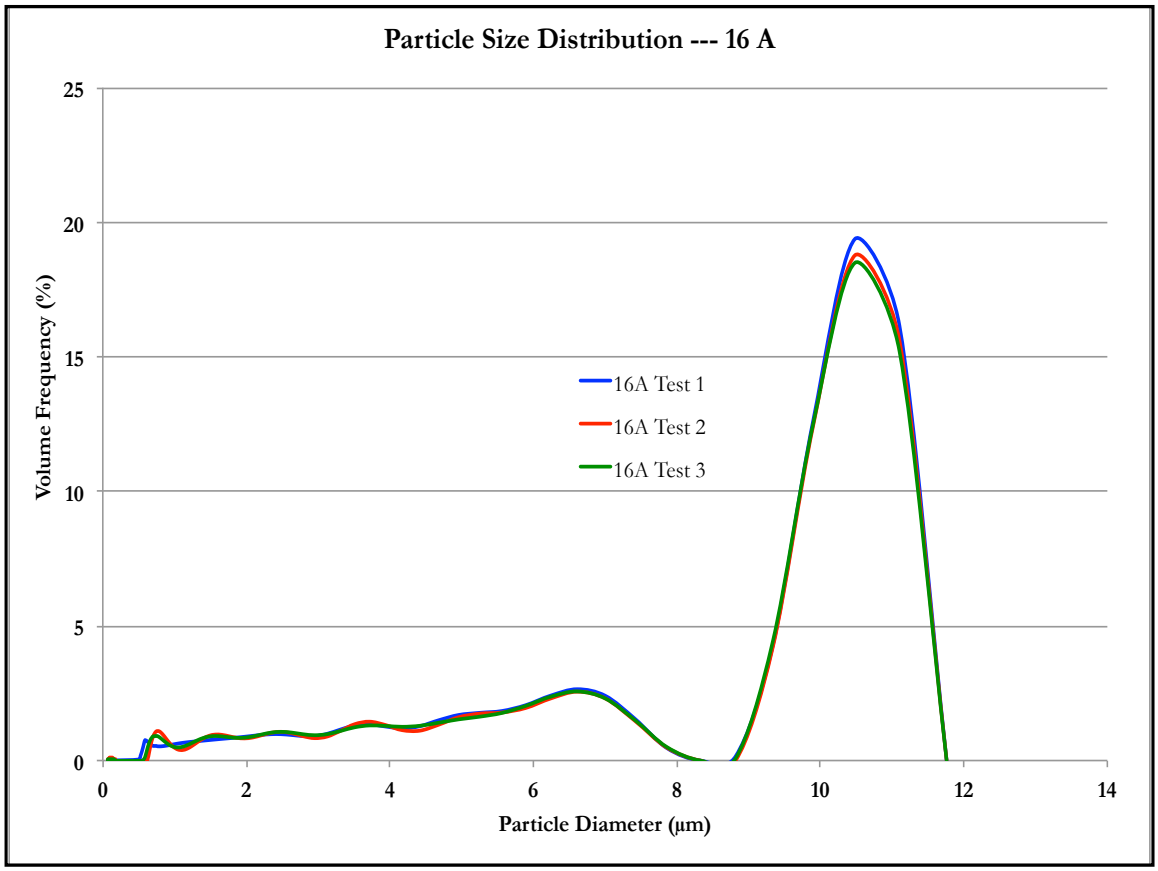

Figure 5.4: Results of 3 particle size measurements are graphed as a function of volume frequency for the 16 A sample. A summary of particle size data for each test is provided in table 5.4.

Table 5.4: Summary report for each 16 A sample Test

Volume Distribution --- 16 A Sample					
	Test 1	Test 2	Test 3	Cumulative Average	
	Diameter (µm)	Diameter (µm)	Diameter (µm)	Diameter (µm)	Std. Dev.
Mean	7.147	7.058	7.039	7.081	0.047
Median	9.422	9.319	9.255	9.332	0.068
Mode	10.48	10.48	10.48	10.48	0.000

The distribution of the 10 A-particle sample exhibits the same overall trend in particle sizes as the 16 A and 25 A samples. However, the distribution for the 10 A sample is shifted to even smaller particle diameters.

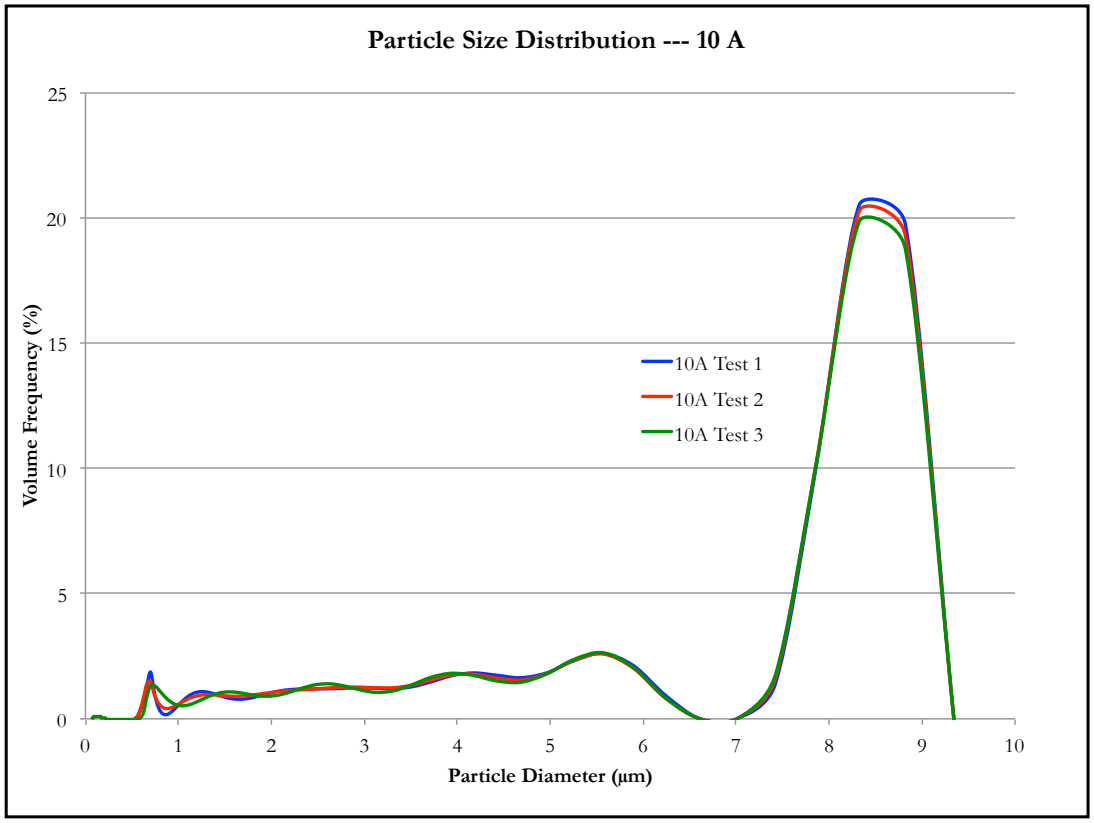

Figure 5.5: Results of 3 particle size measurements are graphed as a function of volume frequency for the 10 A sample. A summary of particle size data for each test is provided in table 5.5.

Table 5.5: Summary report for each 10 A sample Test

Volume Distribution --- 10 A					
	Test 1	Test 2	Test 3	Cumulative Average	
	Diameter (µm)	Diameter (µm)	Diameter (µm)	Diameter (µm)	Std. Dev.
Mean	5.782	5.740	5.662	5.728	0.050
Median	7.686	7.603	7.429	7.573	0.107
Mode	8.326	8.326	8.326	8.326	0.000

The largest peak in the distribution for the 10 A sample can be observed at a diameter of 8.33 µm. A second peak is centered on 5.5 µm and a small, yet well-defined

peak is centered on 0.8 µm. A summary of average particles sizes for each test performed on the 10 A, 16 A, and 25 A samples is included in tables 5.3-5.5.

Overall, the 25 A current generated a particle distribution with the largest diameter particles, while the 10 A current produced the smallest particles. Using a current of 16 A it was found that it is possible to produce particles with a average diameter of 10 µm. The trend in the particle size frequency distribution remained the same between samples, regardless of the intensity of the applied current. The greatest number of counts for each sample occurred at the largest diameter, relative to the rest of the distribution. These relationships are clearly observed in figure 5.6, which shows the average distribution for the 25 A, 16 A, and 10 A samples.

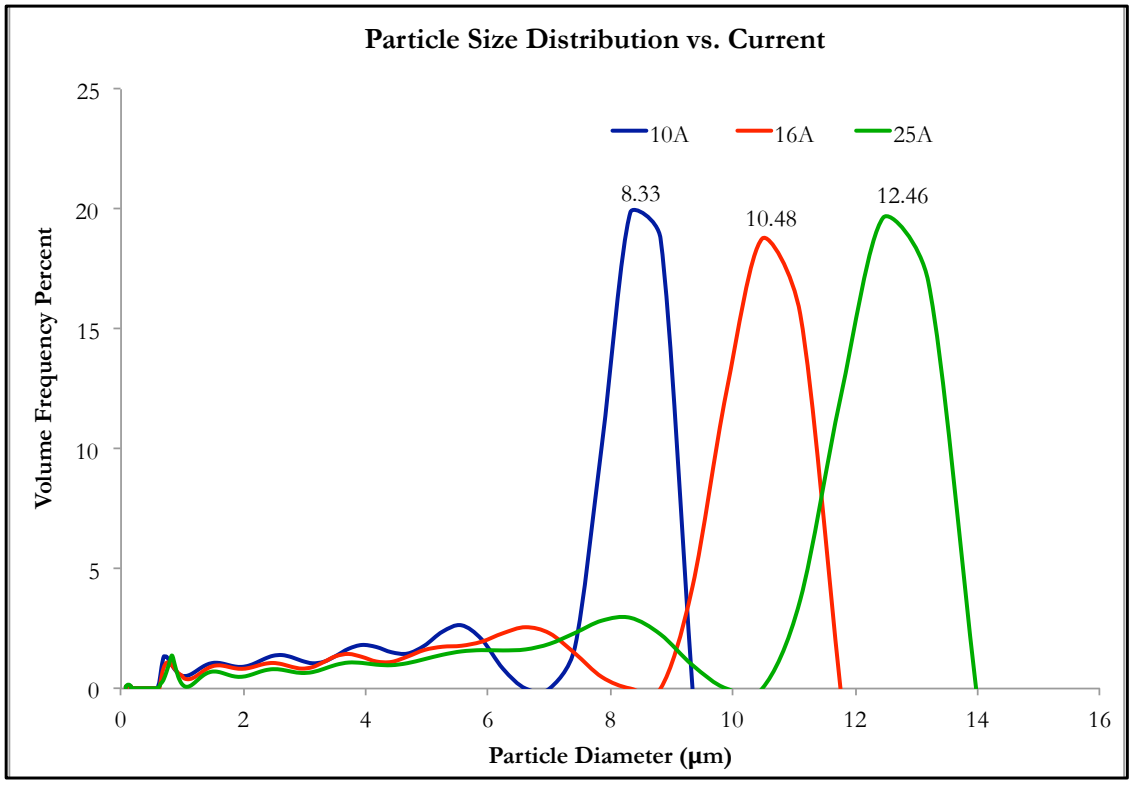

Figure 5.6: Average particle size distribution of each sample (25 A, 16 A, and 10 A)

The Digisizer showed a high degree of reproducibility across the three analyses performed per sample. The results of the analysis reveal an obvious relationship between applied current and particle size. A higher current used during particle fabrication, shifts the particle distribution toward larger diameters. Similarly, a smaller current will produce particles with smaller diameters. For each sample, a large peak over the largest diameter dominated the distribution. Below a value of approximately 0.7X the largest peak diameter, there is a much smaller secondary peak that tapers off towards smaller diameters. A bimodal distribution has been reported in the literature. For example, Cabanillas observed the greatest frequency of particles on the order of 10 μm. The second size group was a range of distributed between 40 and 140 μm. If the lower order particles in this research are taken as a single size group, then the results of this research also indicate a bimodal size distribution using the spark erosion process.

5.4 Particle Imaging

Imaging and energy dispersive X-ray spectroscopy were performed at the University of South Carolina's Electron Microscopy Center (EMC), using the Zeiss Ultra-Plus Field Emission Scanning Electron Microscope (FESEM). Although it is customary to embed particles within an epoxy resin for imaging, the small size of the particles in this research offered an alternative approach. The staff at the EMC recommended that particles be adhered to a small specimen carrier using double-sided and electrically conductive carbon tape. The direct application of the particles to the sample carrier provides better imaging conditions than epoxy mounting and simplifies sample preparation. Figure 5.7 shows an image of the particles mounted to sample carriers using the double stick carbon tape.

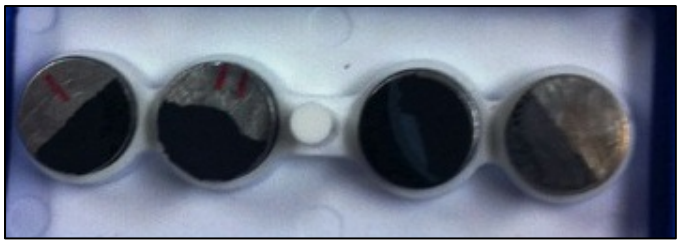

Figure 5.7: Samples prepared for imaging.

Size analysis was performed on the FESEM particle images using ImageJ 1.47 software. ImageJ software can convert and relate pixel count to a known or measured length scale. This made it possible to measure the diameters of the particles using the scale indicated on the FESEM images. The particle sizes shown in the FESEM images agree with the results of the laser light particle size analysis. Additionally, the images show that the spark erosion fabrication method produces highly spherical particles (see figure 5.8.)

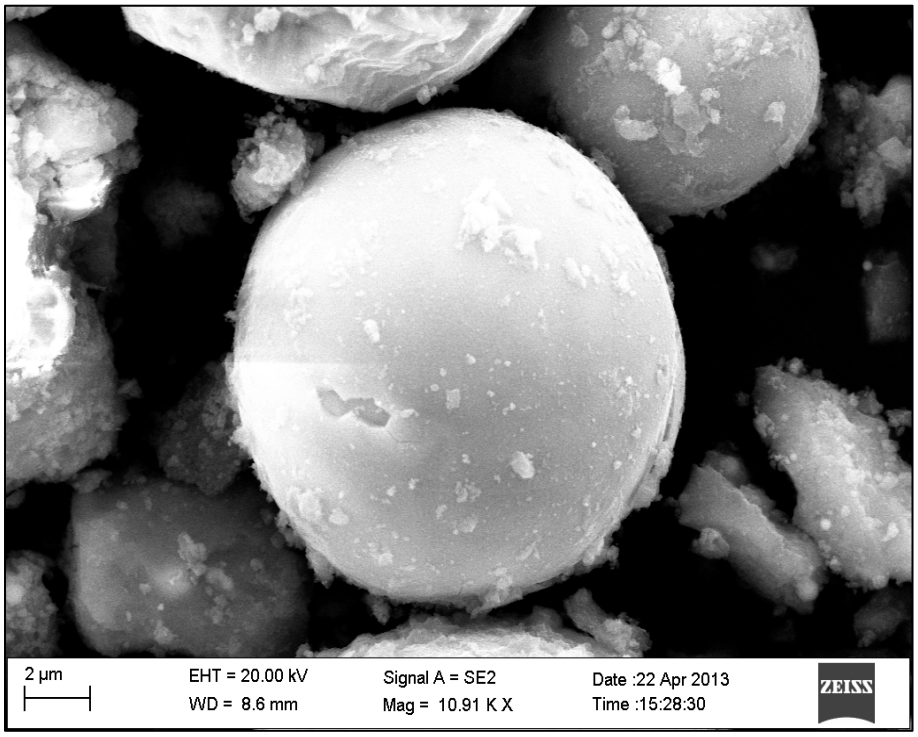

Figure 5.8: Microsphere fabricated at 25 A, with 512 µs pulse duration, and 64 µs pulse off-time. Scale indicated is 2 µm.

Figure 5.9 shows another FESEM image of the 25 A particles. This image includes four spherical particles in the forefront with several smaller particles in the background. Each of the particles would fall within the bounds of the highest frequency peak on the 25 A size distribution. Thus, the particle sizes shown in the image substantiates the distribution reported by laser light particle size analysis.

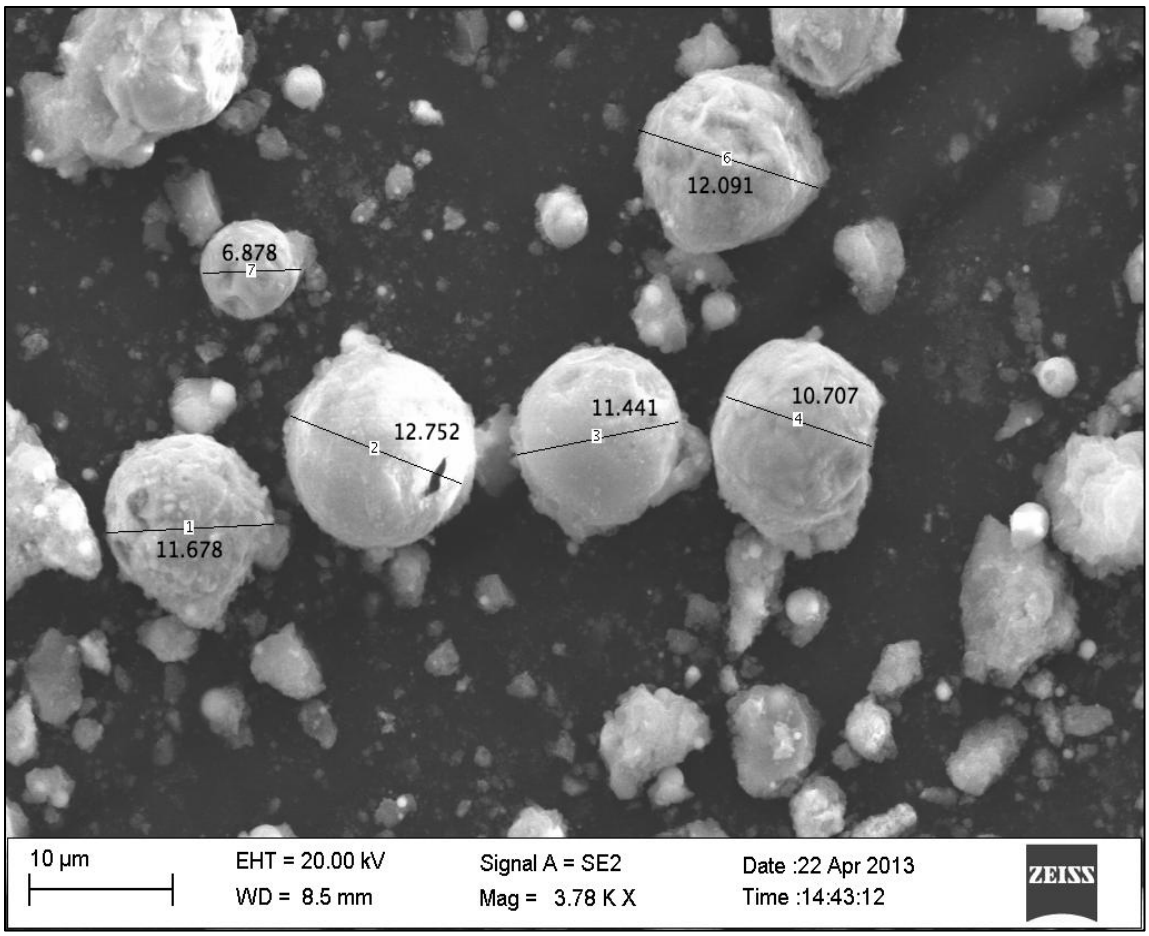

Figure 5.9: Microspheres fabricated at 25 A, with 512 µs pulse duration and 64 µs pulse off-time. Scale indicated is 10 µm.

The particles produced at 16 A conditions also agreed with particle size analysis results and were highly spherical. Figure 5.10 shows several particles produced using a

current of 16 A. The largest particle in the image has a diameter of 10.3 μm and is surrounded by several smaller particles with diameters between 3 μm and 7.6 μm.

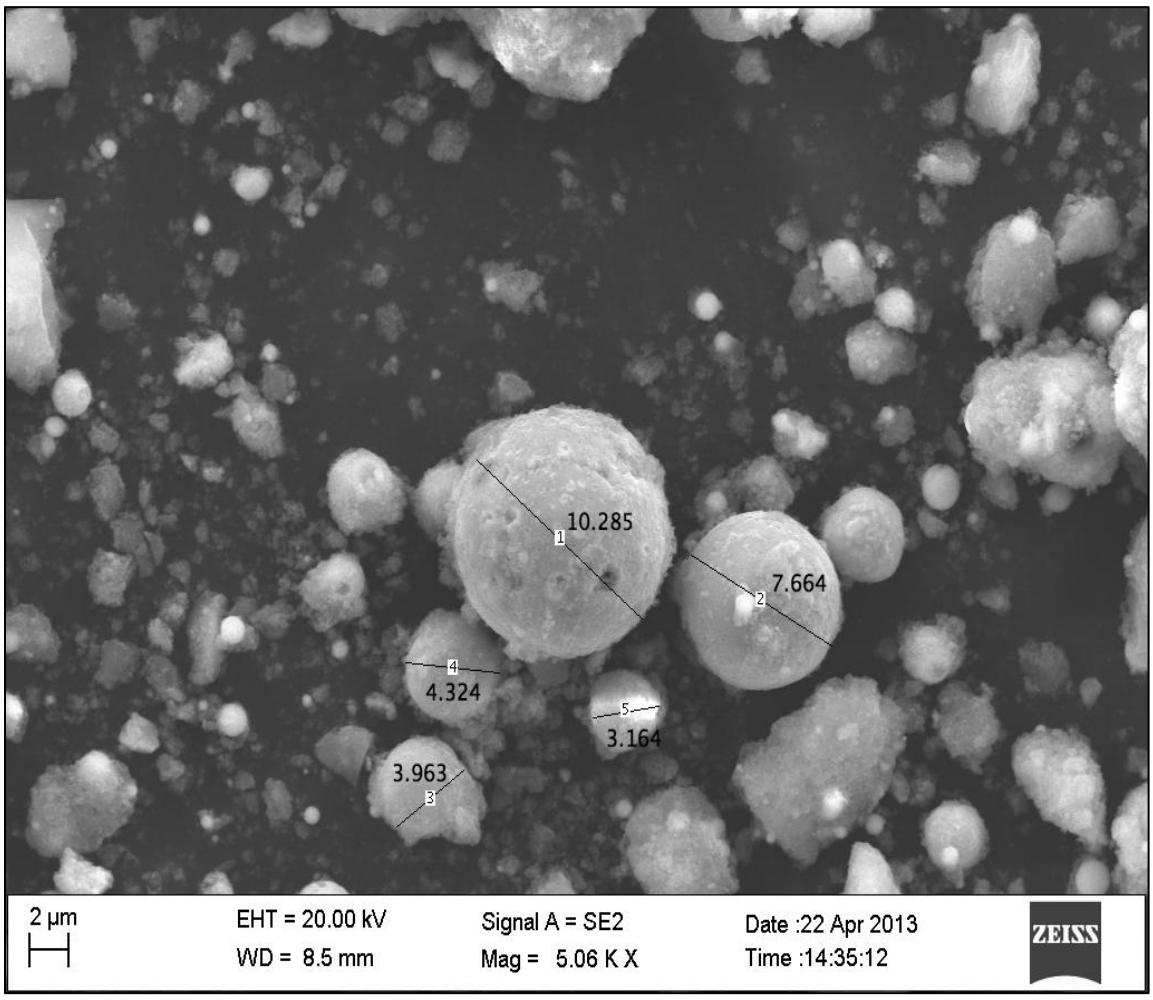

Figure 5.10: Microspheres fabricated at 16 A, with 512 μs pulse duration, and 64 μs pulse off-time. Scale indicated is 2 μm.

Fabricated particles produced using a 10 A current yielded the smallest diameters. Laser light particle size analysis reported the highest diameter frequency was for particles with diameters of approximately 8.3 μm. Figure 5.11 shows an image of several particles from the 10 A-sample. The diameter determined by ImageJ for the largest particle is 8.033 μm, which aligns with the highest peak observed in the particle size distribution

reported by laser light particle size analysis. The smaller particles in the FESEM image also align with the lesser peaks in the size distribution derived from laser light analysis.

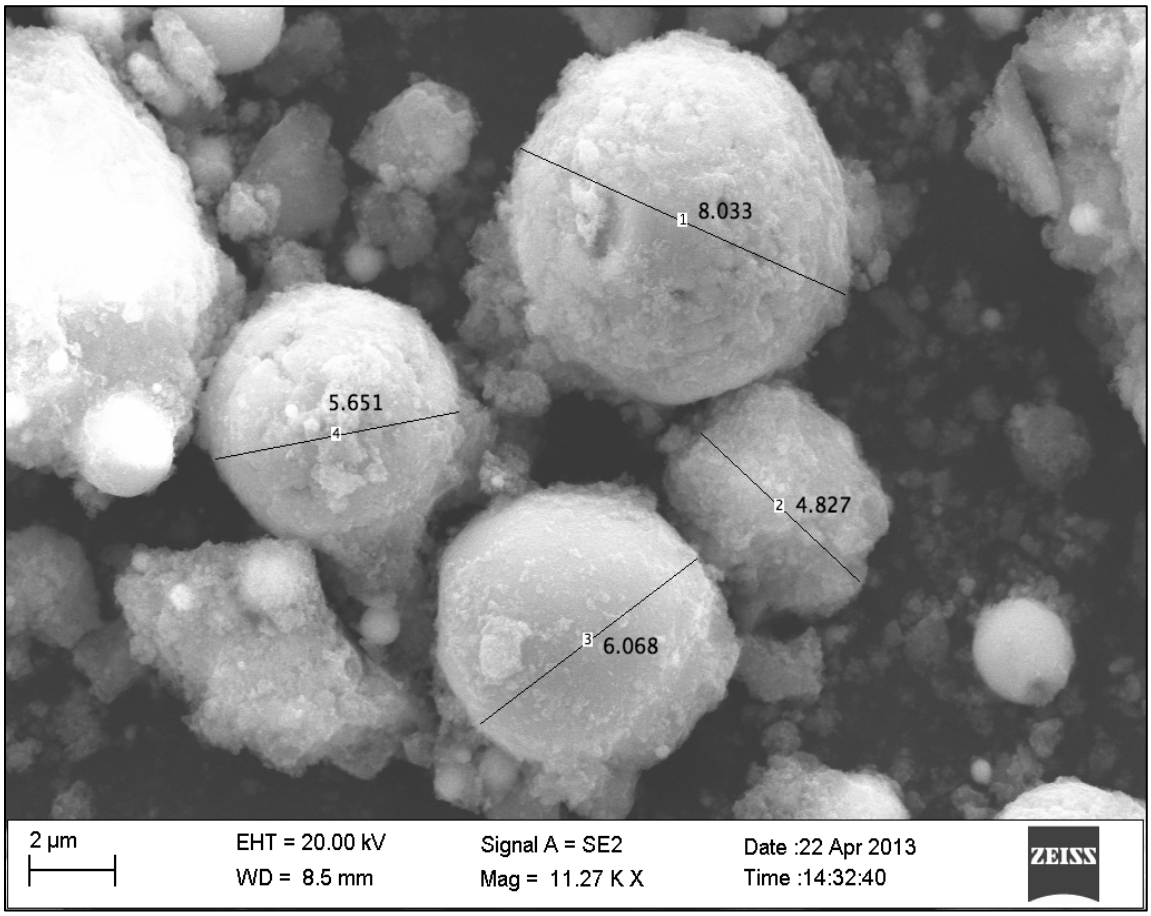

Figure 5.11: Microspheres fabricated at 10 A, with 512 µs pulse duration, and 64 µs pulse off-time. Scale indicated is 2 µm.

For each sample analyzed (25 A, 16 A, and 10 A), the FESEM images substantiate the particle size distribution reported by laser light analysis. The majority of particles are highly spherical in nature; however, some debris particles appear in each of the FESEM images. It is likely that the irregular shaped debris was formed as a result of agglomeration prior to quenching. Under normal operating conditions, the molten material expelled from the electrode forms a sphere due to surface tension and is rapidly quenched in the surrounding dielectric. If the build up of debris in the gap hinders debris

removal, the molten material expelled from the workpiece may interact with existing debris in the gap or recently formed particle debris. This will result in the formation of irregular shaped agglomerate particles.

Although the microstructure of the particles was not studied directly, the FESEM images revealed a high surface porosity in some of the particles. The surface of a particle produced at 25 A is shown in figure 5.12 and reveals a network of pores along the particle surface.

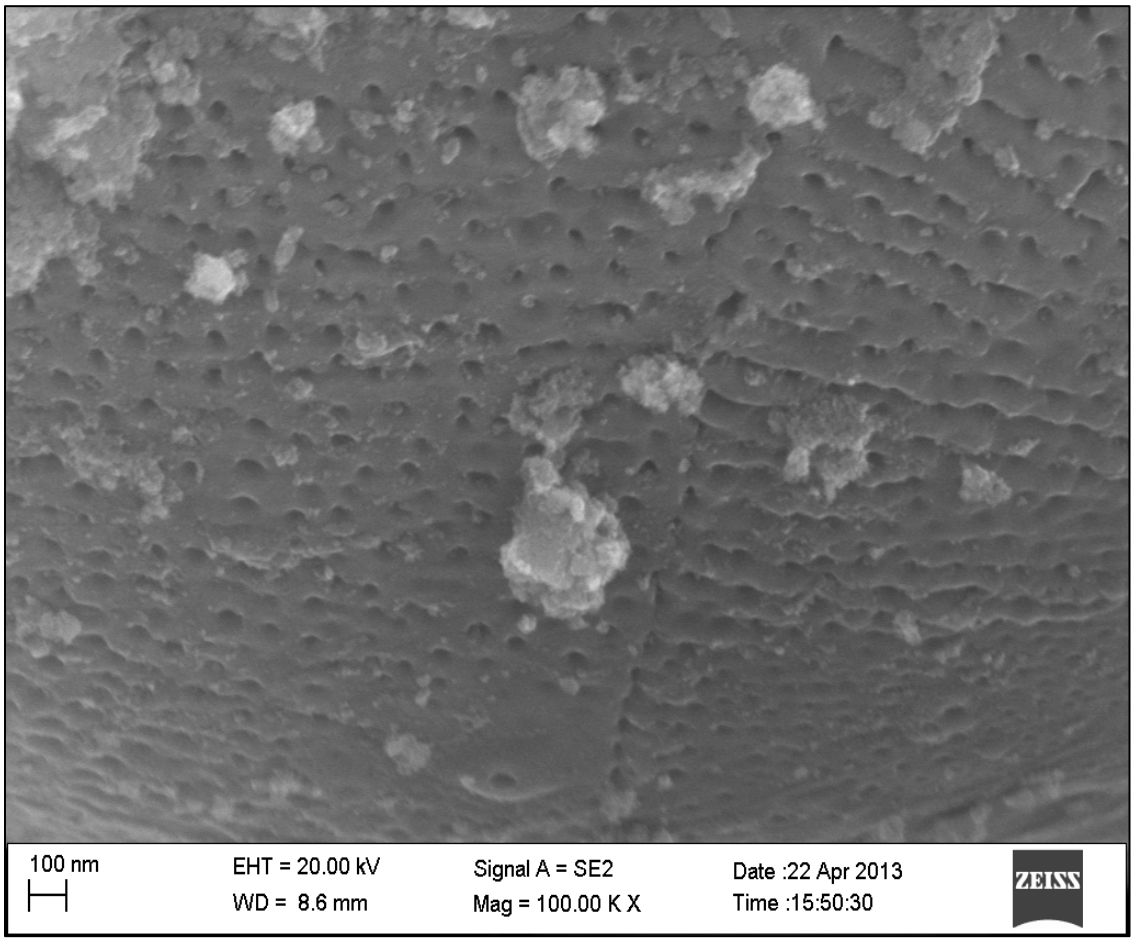

Figure 5.12: Microsphere shows high surface porosity. Scale indicated is 100nm.

The porous surface revealed in the FESEM image suggests a high porosity in the body of the particle, as well. A high porosity and even the existence of a central void are

supported by Cabanillas' research on both iron and U-Mo spark-eroded particles. Using both deionized water and kerosene dielectrics, Cabanillas observed central voids in iron and U-Mo particles [42, 50]. Additionally, the measured density of fabricated particles was much less than the theoretical density of any U-Mo phases. It was determined that the particles were largely UO_2 as a result of a reaction with the dielectric. More importantly, however is that the particle density was still below that of UO_2 (90% of the TD). Based on the literature, it should be realized that particles produced in a water dielectric not only form oxide phases, but also are porous. In terms of the current research, because the oxide phases characteristic of a particle-dielectric reaction were observed (see section 5.5 and 5.6), it is likely the structure of particles would exhibit a moderate body porosity. To evaluate this further, density measurements of the particles were performed using a Micromeritics gas pycnometer. The results are discussed in section 5.7. Future work should include TEM imaging of particle samples or FESEM imaging of cross sections in order to study the central microstructure of particles.

5.5 Energy-Dispersive Spectroscopy

Energy Dispersive Spectroscopy (EDS) was performed on the 16 A sample and is likely representative of the particle composition of both the 10 A and 25 A samples. The purpose of EDS was to determine if the particles produced using spark erosion were contaminated by the tool piece electrode. The workpiece used in this research was 304 Stainless steel and copper was used as the tool piece electrode. If the EDS analysis revealed large amounts of copper beyond the natural composition of the steel electrode, it would serve as proof that the tool electrode had contaminated the particles.

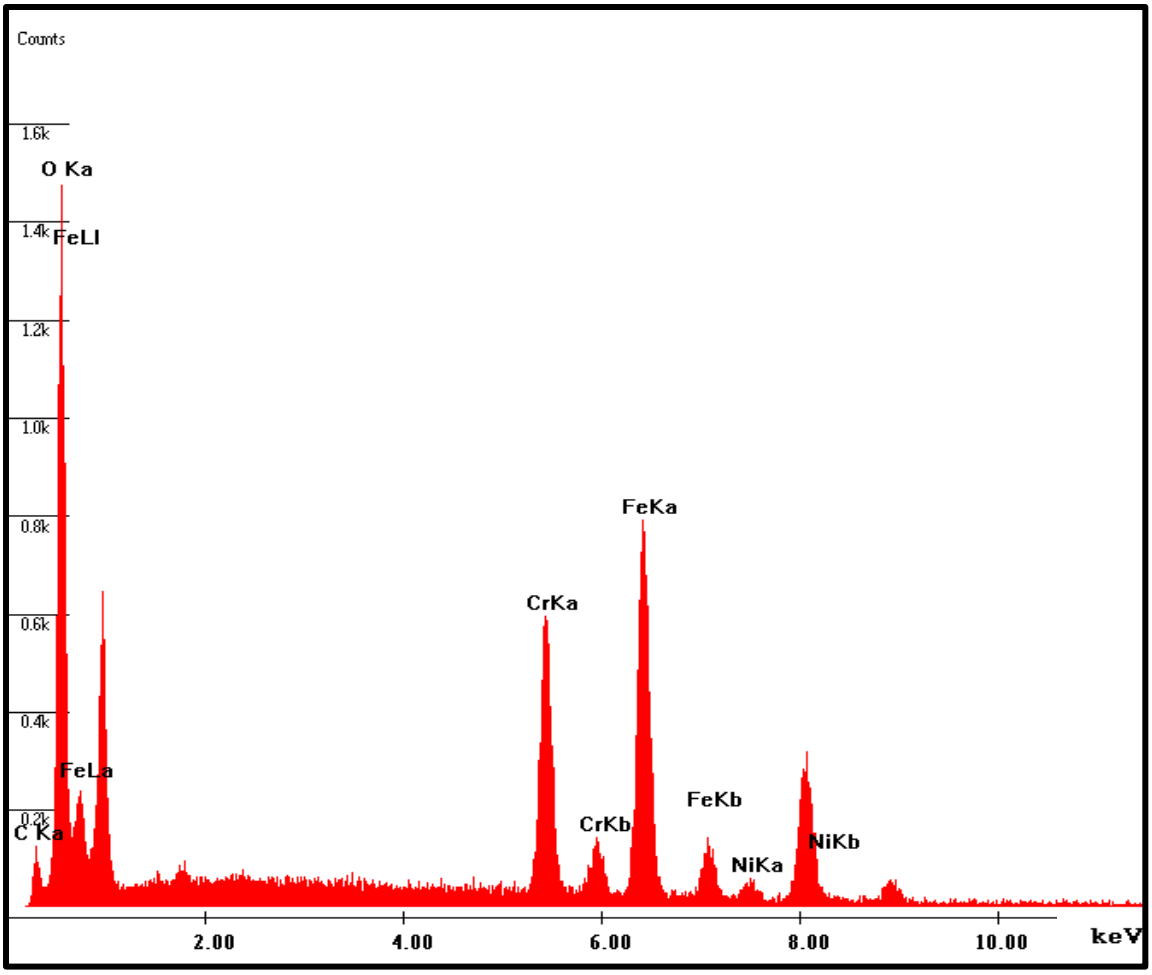

Figure 5.13: EDS spectrum of 16 A particle sample. The counts are shown as a function of energy(keV).

The energy dispersive spectrum for the particle sample shows peaks for carbon, oxygen, chromium, iron, and nickel. Nickel and chromium were both present in the 304 stainless steel electrode by weight percentage of 8-12% and 18-20%, respectively. The carbon identified by the EDS spectrum can be attributed to the conductive carbon tape used for sample preparation. The highest peak in the spectrum is for oxygen. The high oxygen content in the spectrum indicates the presence of oxide phases within the particles. The calculated composition of the sample using the EDS software peak intensity analysis is reported in table 5.6.

Table 5.6: Summary report for each 25 A sample Test

EDS Sample Composition Summary					
Element	Weight %	Atomic %	Net Intensity	Background Intensity	Intensity Error
C	8.10%	15.93%	7.24	2.1	6.61
O	42.54%	62.78%	158.59	4.36	1.15
Cr	15%	6.81%	127.4	8.24	1.33
Fe	32.15%	13.59%	181.18	7.16	1.09
Ni	2.21%	0.89%	8.36	6.08	7.66

It should be noted that copper was not identified in the sample. This indicates that the steel particles did not interact with the copper electrode at any point during fabrication. The choice of using copper as the tool electrode was motivated by the fact that copper has a high thermal diffusivity relative to steel [30]. As a result, it was believed that the melted zone on the copper electrode would be much smaller than that of the steel electrode and could even resolidify during the sparking discharge, yielding no material losses. This was confirmed through EDS because copper was not identified within the sample.

5.6 X-Ray Diffraction Pattern Analysis

Powder X-ray diffraction (XRD) analysis using Cu Kα radiation was performed at the University of South Carolina XRD Facility. A 0.5 g sample was delivered to the staff in a sealed sample container for diffraction analysis. The results were returned in a text data file, which was then analyzed using Match! Phase Identification Software. In order to isolate the peaks in the diffraction pattern, it was necessary to subtract the background noise. Figure 5.14 shows the diffraction pattern as well as identified iron or iron oxide phases.

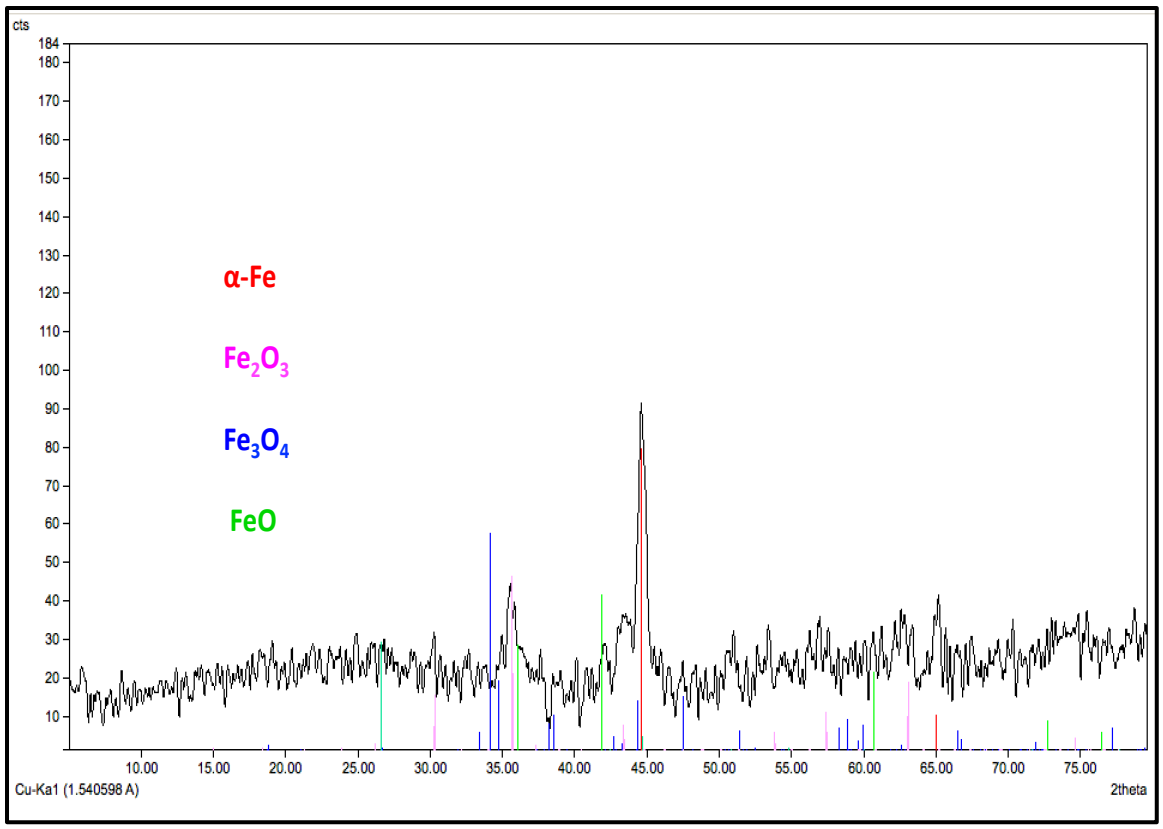

Figure 5.14: Diffraction pattern of sample particles with iron oxide phases indicated.

XRD analysis reveals highly oxidized particles. This confirms the high oxygen content reported by EDS. The largest peak, located at a two-theta value of 44.65 degrees, corresponds to alpha-iron. The intensity of the peak dominated the spectrum and as a result, it was required that the pattern be graphed logarithmically on the Y-axis, corresponding to counts or intensity, to allow all peaks to be seen. The secondary peaks surrounding a two theta value of ~35 degrees provided identification of the iron oxides, Fe_3O_4, Fe_2O_3, and FeO. The approximate amount of each iron oxide phase is given in table 5.7. These amounts were obtained in the Match! Software, using a module in which composition amounts are related to the ratios of peak intensities.

Table:5.7: Composition of matched phases for figure 5.14.

Matched Phases		
Index	Composition	Amount
A	Fe_3O_4	37.50%
B	Fe_2O_3	30.20%
C	FeO	17.30%
D	Fe	15.10%

The calculated quantity of each phase assumes that the particle composition is comprised entirely of the selected phases. Therefore, the results in table 5.7 do not provide a full picture, given that a highly heterogeneous composition is expected [42]. The values in the table should instead only be used to reference the amounts of each iron oxide relative to one another. Upon inspection, it was determined that the fabricated particles were magnetic. The identified phases alpha-iron, Fe_3O_4, and Fe_2O_3 are highly magnetic which supports a positive identification of iron phases identified through XRD. Future work should investigate the possibility of particle retrieval from the dielectric by magnet.

Beyond the pronounced secondary peak, composition identification grew increasingly difficult due to the abundance of matched phases. The peaks for Cr_2FeO_4 and Cr_2NiO_4 provided the best match to the diffraction spectrum aside from the previously discussed iron oxide phases (see figure 5.15). Additionally, the extreme quenching process, experienced by the molten debris, presents another opportunity for oxygen to enter the particle composition.

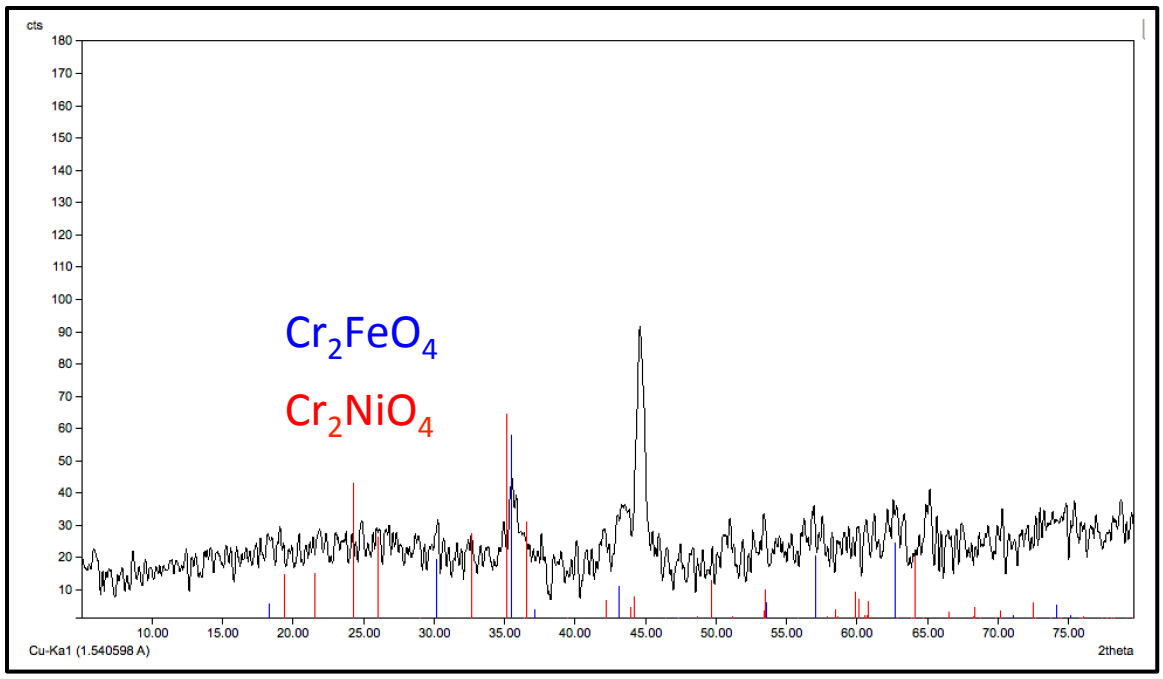

Figure 5.15: Diffraction pattern of sample particles with peaks labeled for observed chromium and nickel phases.

It is likely that the true particle composition consists of numerous other oxide compounds and phases. The formation of the identified oxides can be explained by the hydrolysis of water dielectric during sparking. As the oxygen and hydrogen bonds break down, a large quantity of oxygen ions become available for reaction with the molten material expelled from the electrode. It is reasonable to assume that the violent and non-equilibrium conditions associated with the interaction between the deionized water and molten steel allowed for the formation of a complex multicomponent system. Additionally, the rapid quenching and non-equilibrium cooling likely resulted in further phase transformations. Future particle analysis should include cross sectional imaging and EDS measurements at numerous locations throughout the particle in order to provide a better understanding of composition and microstructure.

5.7 Density Measurements

Density measurements were performed using a Micromeritics Accupyc II 1340 pycnometer. The instrument determines density and volume by measuring the pressure change of gas within calibrated volumes. The sample is placed in one of two chambers within the device. Pressurized gas then fills the sample volume to a specified pressure (in this case, 19.5 psig). The gas is then permitted to expand and fill a second chamber. A transducer measures the pressure drop in the sample chamber and the ideal gas law is used to determine the volume of the sample. Prior to the density measurements, the system was calibrated such that the volume of the chambers and sample holder could be determined. Helium or other chemically inert gases can be used as the fill gas. When the gas is changed, another calibration should be performed on the system. For this measurement, high purity argon gas was used and the chamber volumes were calibrated. The mass of the sample was entered prior to the analyses so that the system could automatically determine the density of the sample. A 0.118 g particle sample was placed in the 0.1 cm^3 insert cup and ten measurements were performed. The results are shown in in figure 5.16. The average of the ten density measurements is 5.00 g/cm^3.

The 304 SS workpiece electrode had a density of 8.03 g/cm^3. Assuming the particle composition was consistent with that of the workpiece, then the particle sample is approximately 62.3% TD. However, given the results of XRD and EDS, the composition of the samples consisted of various oxide phases. The identified oxides have densities between 4.88 g/cm^3 and 6.16 g/cm^3. The alpha-iron identified through XRD has a density of 7.86 g/cm^3. Without complete determination of the particle phases, it is difficult to predict the degree of porosity throughout the samples. However, given the initial workpiece density as well as the phases identified through XRD, it is clear that the

particles exhibit a substantial degree of porosity that would benefit from further inspection.

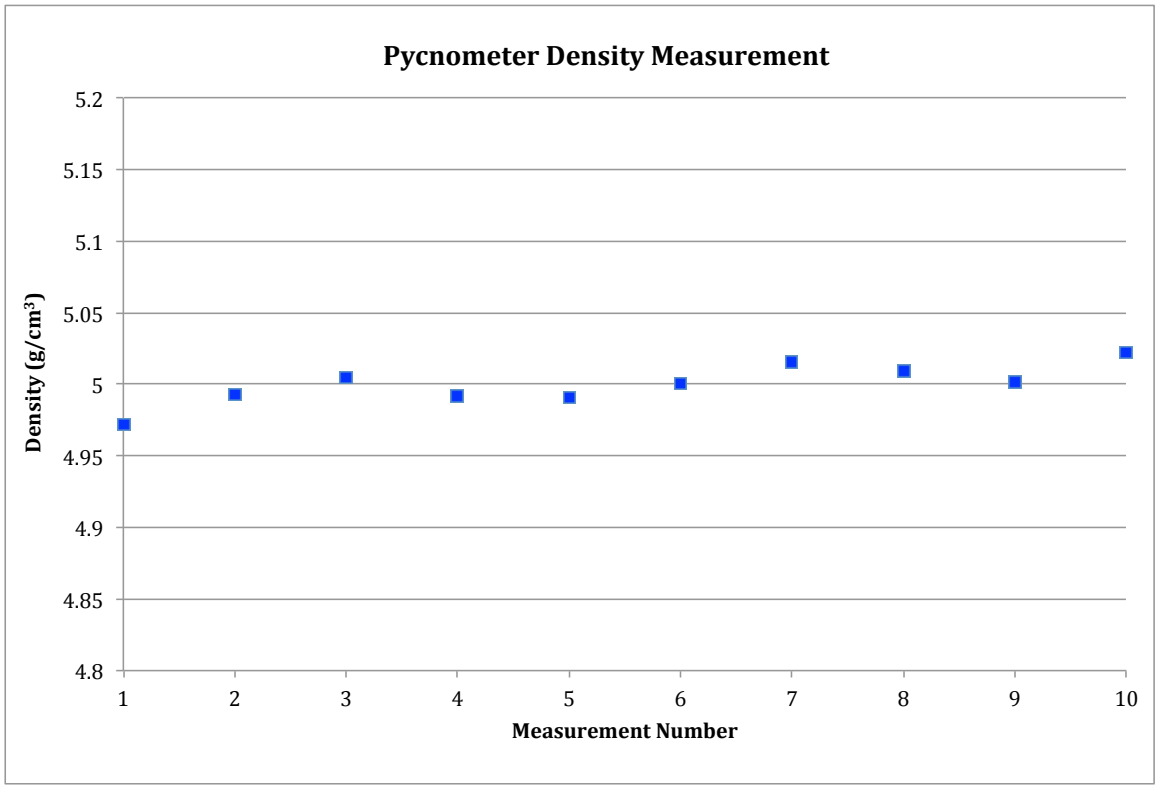

Figure 5.16: Results of 10 density measurements.

CHAPTER 6

CONCLUSIONS AND FUTURE WORK

6.1 GENERAL CONCLUSIONS

The results of this work suggest that spark erosion machining is a viable method of producing micron-sized fuel particles. The stainless steel surrogate particles produced through the spark erosion process were representative of fuel particles required in advanced dispersion fuel designs. In order to achieve competitive fissile loading, such fuel designs must utilize a distribution of multiple fuel particle sizes. Because the volume loading increases with the ratio of large particle diameter to that of the smaller particle diameter, it was necessary to identify a particle fabrication process capable of producing spheres as small as 10 μm.

To qualify the spark erosion process, fabrication experiments were designed using a CT Electromechanica spark erosion device. The retrieval of particles from the dielectric and catchment tank required the development of a vacuum filtration system, which utilized a polycarbonate membrane filter. The filtration system was extremely successful in filtering and retrieving particles from the dielectric medium. If future work requires a narrow range of particle sizes, a series of filtrations is suggested using filters of varying particle retention capacity. Additionally, if work is continued using steel or iron-based workpiece electrodes, magnetic particle retrieval should be attempted given that the fabricated particles in this work were found to be highly magnetic.

The evaluation of the spark erosion process was ultimately based on its ability to produce micron-sized particles. Using parameters from the literature as a guide, conditions and experimental parameters were selected that were believed would produce particles 10 μm in size. Three current intensities were tested, 10 A, 16 A, and 25A. In each experiment, a high sparking frequency was employed, marked by both a short pulse length and pulse width (512 μs and 64 μs, respectively).

Fabricated particles were characterized to determine size distributions as well as the composition. Laser light particle size analysis was used to find the size distribution for samples of each current intensity. Particle sizes were confirmed through FESEM imaging. The results of size analysis reveal a similar trend in particle size for all samples. If the smaller sized particles are collected into a single group, the distribution can be considered bimodal. The greatest volume frequency belonged to particles with the largest diameter in the distribution. The remaining particle sizes occurred with far less frequency and were distributed below approximately 0.7x the value belonging to most frequent particle diameter (the largest peak in the distribution). For the 25 A sample, the greatest frequency of particles occurred at a diameter of 12 μm. The mode of the 16 A sample occurred for a diameter of 10μm. For the 10 A sample, 8μm was the mode diameter.

EDS and XRD analyses were also performed to determine the composition of the particles. EDS results reveal high oxygen content in the particles. Similarly, the XRD pattern showed the particles formed oxides during particle formation. This indicates that the deionized water dielectric reacted with the molten debris. The research confirms that the dielectric must be chosen with regards to the compositional requirements of the

desired particles, as the chemical composition dielectric will control the fabricated particle composition.

Density measurements performed using gas pycnometry indicate that the particles had a density of 5.00 g/cm^3. The stainless steel workpiece electrode had a density of 8.03 g/cm^3. Assuming the particle composition was consistent with that of the workpiece, then the particle sample is approximately 62.3% TD. However, given the results of XRD and EDS, the composition of the samples consisted of various oxide phases. Without complete determination of the particle phases, it is difficult to accurately predict the degree of porosity throughout the samples. However, it is clear that the particles exhibit a substantial degree of porosity that would benefit from further inspection.

Additionally, the spark erosion process was evaluated for production capabilities, including particle yield. The results of the tests show that the particle fabrication rate remained linear with increasing experiment duration. For 16 A experiments maintained for 3 hours, the average yield was ~0.6 g. As a result, it can be said that the spark erosion device and method used in this research would not generate a significant yield of particles in a timely manner for production-scale applications. If the electrode diameter could be increased, the particle yield and fabrication rate would also increase. However, the retainer for the workpiece and tool electrode currently limit the electrode diameter to approximately 0.5 in. Yield would also increase if particle retention in the system could be reduced. It was determined that the greatest retention of particles occurred in the catchment tank. A smaller tank would provide less surface area for particles to adhere to. Additionally, use of the current spark erosion device for the production of nuclear fuel particles will require a redesigned catchment tank to minimize the volume of dielectric

required to fully submerge the electrodes. The spark erosion process and the subsequent particle filtration generate a large quantity of liquid waste, which would need to be minimized to address disposal issues associated with mixed and liquid forms of radioactive waste.

6.2 Recommendations for Future Work

Future efforts should focus on understanding the effect system parameters have on particle microstructure and composition. Although a reaction between the particles and dielectric was shown to produce oxides, a formal understanding of particle microstructure is required.

The particle microstructure should be investigated in more detail through additional imaging. A porous particle surface was revealed in an FESEM image, which suggested a high porosity in the body of the particle, as well. Pycnometry measurements reveal that the density of the particles is 5.00 g/cm^3. Relative to the density of the 304 SS workpiece, the particles have a high degree of porosity. However, the density of the sample also supports the XRD and EDS results that that suggested the debris formed oxide phases. Although the phases identified through XRD have densities lower than that of the starting workpiece, they are still larger than the density value obtained for the fabricated particles. This indicates that even if the particles formed oxides, they also developed a porous microstructure. Additional particle imaging should be performed on cross-sectioned particles in order to study the central microstructure. At the same time, EDS analysis could be performed at locations throughout the particle in order to determine the degree of heterogeneity in particle composition. This follow up EDS analysis could also be used to verify the carbon content detected in this research. It is

likely that the carbon was due to the carbon tape used to mount particles to the sample holder. However, EDS analysis on resin mounted particles rather than carbon adhered particles will confirm or disprove the measured carbon content in the particles.

Ideally, future spark eroded work should utilize a metallic workpiece electrode, rather than alloy. This would greatly simplify the determination of particle composition and would improve the accuracy of the XRD analysis. Accurate identification of phases in the particle would encourage a greater understanding of the microstructure and composition. This would allow for a more meaningful discussion of the environmental conditions associated with particle formation.

Other system parameters could also be investigated to determine their impact on the fabricated particle size distribution. The effect of a shorter current pulse length in exchange for a larger current intensity could produce interesting results. Similarly, a combination of increased current pulse length and smaller current intensity could be investigated to determine the impact on the particle size distribution.

An increased understanding of the particle microstructure is required before useful suggestions can be provided for the extension of this process to actual fuel particle production. If surrogate particles produced in a water dielectric are found to have central voids, it may prevent the use of water dielectrics in the development of fuel particles. Instead it may prove more advantageous to use kerosene as the dielectric to ensure solid particles are formed. If oxide particles are desired, UC particles (or other carbides) could be reduced in a CO environment in order to yield UO_2. Arcing in an inert gas dielectric will eliminate the issue of reacted particles entirely. In this case, particles can maintain

the composition of the starting workpiece electrode material. Fuel particles produced in this manner could be subjected to further oxidation to yield desired compositions.

REFERENCES

[1] Goldner, Frank. "Development Strategy for Advanced LWR Fuels with Enhanced Accident Tolerance." PowerPoint presentation, Nuclear Energy Advisory Committee Meeting, US Department of Energy, Washington D.C., June 12, 2012.

[2] McGEARY R.K. 1961. Mechanical packing of spherical particles. *Journal of the American Ceramic Society* 44: 513-522.

[3] VAIDYA V.N. 2008. Status of sol–gel process for nuclear fuels. *Journal of Sol-Gel Science and Technology* 46: 369-381.

[4] CARREY J., RADOUSKY H.B. & BERKOWITZ A.E. 2004. Spark-eroded particles: Influence of processing parameters. *Journal of applied physics* 95: 823-829.

[5] FROST B.R.T., R.W. CAHN, P. HAASEN & E.J. KRAMER 2005. *Nuclear materials*. Wiley-VCH.

[6] Meyer, M.K. "High Burnup Fuels." Presentation, GCEP Fission Workshop, Massachusetts Institute of Technology, November 29, 2007.

[7] MURANAKA R.G. 1983. Conversion of research reactors to low-enrichment uranium fuels. *IAEA Bulletin* 25: 18-20.

[8] OLANDER D. 2008. Fission-enhanced diffusion in dispersion fuels. *Journal of Nuclear Materials* 372: 94-105.

[9] SNELGROVE J.L., HOFMAN G.L., TRYBUS C.L. & WIENCEK T.C. 1996. Development of very-high-density fuels by the RERTR program. Proceedings of the International Meeting on Reduced Enrichment for Research and Test Reactors, Seoul, Korea: 7-10.

[10] IAEA. 2003. *Development Status of Metallic, Dispersion and Non-oxide Advanced and Alternative Fuels for Power and Research Reactors*. Report.

[11] VAN DUYN L.B. 2003. Evaluation of the mechanical behavior of a metal-matrix dispersion fuel for Plutonium burning. Georgia Institute of Technology, Nuclear Engineering. <http://smartech.gatech.edu/jspui/bitstream/1853/5301/vanduyn_lee_b_200312.pdf>.

[12] FURNAS C.C. 1931. Grading Aggregates-I.-Mathematical Relations for Beds of Broken Solids of Maximum Density. *Industrial & Engineering Chemistry* 23: 1052-1058.

[13] FINLAY M.R., HOFMAN G.L. & SNELGROVE J.L. 2004. Irradiation behavior of uranium silicide compounds. *Journal of nuclear materials* 325: 118-128.

[14] DING S., WANG Q. & HUO Y. 2010. Mechanical behaviors of the dispersion nuclear fuel plates induced by fuel particle swelling and thermal effect II: Effects of variations of the fuel particle diameters. *Journal of Nuclear Materials* 397: 80-91.

[15] JIANG Y., WANG Q., CUI Y., HUO Y., DING S., ZHANG L. & LI Y. 2011. Prediction of the micro-thermo-mechanical behaviors in dispersion nuclear fuel plates with heterogeneous particle distributions. *Journal of Nuclear Materials* 418: 69-79.

[16] VASUDEVAMURTHY G. 2007. Composite nuclear fuel fabrication methodology for gas fast reactors. University of South Carolina, *Nuclear Engineering.*

[17] SAVCHENKO A., KONOVALOV I., VATULIN A., MOROZOV A., ORLOV V., UFEROV O., ERSHOV S., LAUSHKIN A., KULAKOV G. & MARANCHAK S. 2007. Dispersion type zirconium matrix fuels fabricated by capillary impregnation method. *Journal of nuclear materials* 362: 356-363.

[18] HUNT R.D. & COLLINS J.L. 2004. Uranium kernel formation via internal gelation. *Radiochimica Acta/International journal for chemical aspects of nuclear science and technology* 92: 909-915.

[19] KUNIEDA M., LAUWERS B., RAJURKAR K.P. & SCHUMACHER B.M. 2005. Advancing EDM through fundamental insight into the process. *CIRP Annals-Manufacturing Technology* 54: 64-87.

[20] Harding, Henry. "Disintegrating or removing metallic material." Patent 2592894. April 1952.

[21] LAZARENKO B.R. 1943. To invert the effect of wear on electric power contacts. Dissertation of the All-Union Institute for Electro Technique in Moscow/CCCP (in Russian).

[22] BERKOWITZ A.E. & WALTER J.L. 1987. Spark erosion: A method for producing rapidly quenched fine powders. *Journal of Materials Research* 2: 277-288.

[23] CHAMPAGNE B., ANGERS R. & FISET M. 1984. Characteristics of powders produced by the rotating electrode process. *Met. Powder Rep.* 39: 267-270.

[24] PALATNIC L.S. & LIULICHEV A.N. 1958. Investigation of the Temperature in the Vapor Phase Occurring during the Electrical Spark Treatment of Metals. *Soviet Phys.-Tech. Phys* 1: 818.

[25] ALBINSKI K., MUSIOL K., MIERNIKIEWICZ A., LABUZ S. & MALOTA M. 1996. The temperature of a plasma used in electrical discharge machining. *Plasma Sources Science and Technology* 5: 736.

[26] HASHIMOTO G. & KUNIEDA M. 1997. Spectroscopic analysis of temperature variation of EDM arc plasma. *Journal of JSME B* 31: 32-40.

[27] NATSU W., OJIMA S., KOBAYASHI T. & KUNIEDA M. 2004. Temperature distribution measurement in EDM arc plasma using spectroscopy. *JSME International Journal Series C* 47: 384-390.

[28] ECKMAN P.K. & WILLIAMS E.M. 1960. Plasma dynamics in an arc formed by low-voltage spark over of a liquid dielectric. *Applied Scientific Research, Section B* 8: 299-320.

[29] XIA H., KUNIEDA M. & NISHIWAKI N. 1996. Removal amount difference between anode and cathode in EDM process. *International journal of electrical machining* 1: 45-52.

[30] SAITO N. & KOBAYASHI K. 1967. Machining Principle and Characteristics of Electric Discharge Machining. *Mitsubishi Denki Giho* 41: 1222-1230.

[31] HOCKENBERRY T.O. & WILLIAMS E.M. 1967. Dynamic evolution of events accompanying the low-voltage discharges employed in EDM. *Industry and General Applications, IEEE Transactions on* 302-309.

[32] YOSHIDA M. & KUNIEDA M. 1998. Study on the distribution of scattered debris generated by a single pulse discharge in EDM process. *International journal of electrical machining* 3: 39

[33] ZHANG Q.H., DU R., ZHANG J.H. & ZHANG Q.B. 2006. An investigation of ultrasonic-assisted electrical discharge machining in gas. *International Journal of Machine Tools and Manufacture* 46: 1582-1588.

[34] JILANI S.T. & PANDEY P.C. 1984. Experimental investigations into the performance of water as dielectric in EDM. *International Journal of Machine Tool Design and Research* 24: 31-43.

[35] JESWANI M.L. 1981. Electrical discharge machining in distilled water. *Wear* 72: 81-88.

[36] MOHD ABBAS N., SOLOMON D.G. & FUAD BAHARI M. 2007. A review on current research trends in electrical discharge machining (EDM). *International Journal of Machine Tools and Manufacture* 47: 1214-1228.

[37] ZHAO F., LU Z. & WANG H. 2005. Research on effecting mechanism of particles in powder-mixed EDM. *JOURNAL-DALIAN UNIVERSITY OF TECHNOLOGY* 45: 668.

[38] MING Q.Y. & HE L.Y. 1995. Powder-suspension dielectric fluid for EDM. *Journal of materials processing technology* 52: 44-54.

[39] YIH-FONG T. & FU-CHEN C. 2005. Investigation into some surface characteristics of electrical discharge machined SKD-11 using powder-suspension dielectric oil. *Journal of materials processing technology* 170: 385-391.

[40] ZHAO W.S., MENG Q.G. & WANG Z.L. 2002. The application of research on powder mixed EDM in rough machining. *Journal of materials processing technology* 129: 30-33.

[41] TZENG Y.-F. & LEE C.-Y. 2001. Effects of powder characteristics on electrodischarge machining efficiency. *The International Journal of advanced manufacturing technology* 17: 586-592.

[42] CABANILLAS E.D., LÓPEZ M., PASQUALINI E.E. & CIRILO LOMBARDO D.J. 2004. Production of uranium–molybdenum particles by spark-erosion. *Journal of nuclear materials* 324: 1-5.

[43] VASUDEVAMURTHY G. & KNIGHT T.W. 2007. Effect of system parameters on size distribution of 304 stainless steel particles produced by electrical discharge mechanism. *Materials Letters* 61: 4872-4874.

[44] SVEDBERG T. & RINDE H. 1924. The ultra-centrifuge, a new instrument for the determination of size and distribution of size of particle in microscopic colloids. *Journal of the American Chemical Society* 46: 2677-2693.

[45] CHAMPAGNE B. & ANGERS R. 1980. Size distribution of powders atomized by the rotating electrode process. *Modern Development in Powder Metallurgy* 12: 83-104.

[46] ANGERS R. 1992. Centrifugal Atomization Influence of Process Parameters on Size Distribution. *Advances in Powder Metallurgy & Particulate Materials--1992*. 1: 79-88.

[47] CABANILLAS E.D. 2007. TEM observations of particles obtained by electro-erosion in kerosene. *Journal of materials science* 42: 3155-3160

[48] SLADE S.B., BERKOWITZ A.E. & PARKER F.T. 1991. Preparation and properties of noninteracting spherical magnetic particles. *Journal of Applied Physics* 69: 5127-5129.

[49] DIGISIZER S. 2002. 5200 Operators Manual 520-42801-01. *Micromeritics Instrument Corporation, Norcross, GA (Aug. 2002)*

[50] CABANILLAS E.D., PASQUALINI E.E., LÓPEZ M., CIRILO D., DESIMONI J. & MERCADER R.C. 2001. Morphology and phase composition of particles produced by electro-discharge-machining of iron. *Hyperfine interactions* 134: 179-185.

APPENDIX A: PEAK SUMMARY FROM PARTICLE SIZE DISTRIBUTIONS

(See section 5.3)

Table A.1: Peak Summary Report for 25 A Sample

Peaks Summary Report (25 A Sample)		
Test 1		
Peak #	% of Distribution	Mean Diameter
1	8.9	3.415
2	22.6	6.866
3	56.8	12.46
Test 2		
Peak #	% of Distribution	Mean Diameter
1	7.7	1.499
2	5.1	2.816
3	6.1	4.093
4	7.3	5.619
5	14.7	7.811
6	55.1	12.4
Test 3		
Peak #	% of Distribution	Mean Diameter
1	5.3	0.841
2	6.5	3.767
3	22.9	6.855
4	53.5	12.4

Table A.2: Peak Summary Report for 16 A Sample

Peaks Summary Report (16 A Sample)		
Test 1		
Peak #	% of Distribution	Mean Diameter
1	17.9	1.777
2	7.3	3.849
3	19.6	6.254
4	50.9	10.42
Test 2		
Peak #	% of Distribution	Mean Diameter
1	7.3	0.828
2	7.9	1.564
3	6.6	2.482
4	8.3	3.736
5	17.5	6.035
6	51	10.42
Test 3		
Peak #	% of Distribution	Mean Diameter
1	7.1	0.79
2	7.7	1.475
3	7.8	2.427
4	7.2	3.643
5	18.9	5.916
6	50.7	10.41

Table A.3: Peak Summary Report for 10 A Sample

Peaks Summary Report (10 A Sample)		
Test 1		
Peak #	% of Distribution	Mean Diameter
1	6.2	0.695
2	9.1	1.28
3	13.5	2.463
4	9.7	4.087
5	9.8	5.499
6	51.7	8.39
Test 2		
Peak #	% of Distribution	Mean Diameter
1	6.6	0.704
2	8.1	1.247
3	13.5	2.329
4	10.8	3.975
5	9.6	5.488
6	51.4	8.381
Test 3		
Peak #	% of Distribution	Mean Diameter
1	8.5	0.794
2	9.8	1.515
3	9.6	2.568
4	10.7	3.969
5	9.7	5.491
6	50.5	8.375